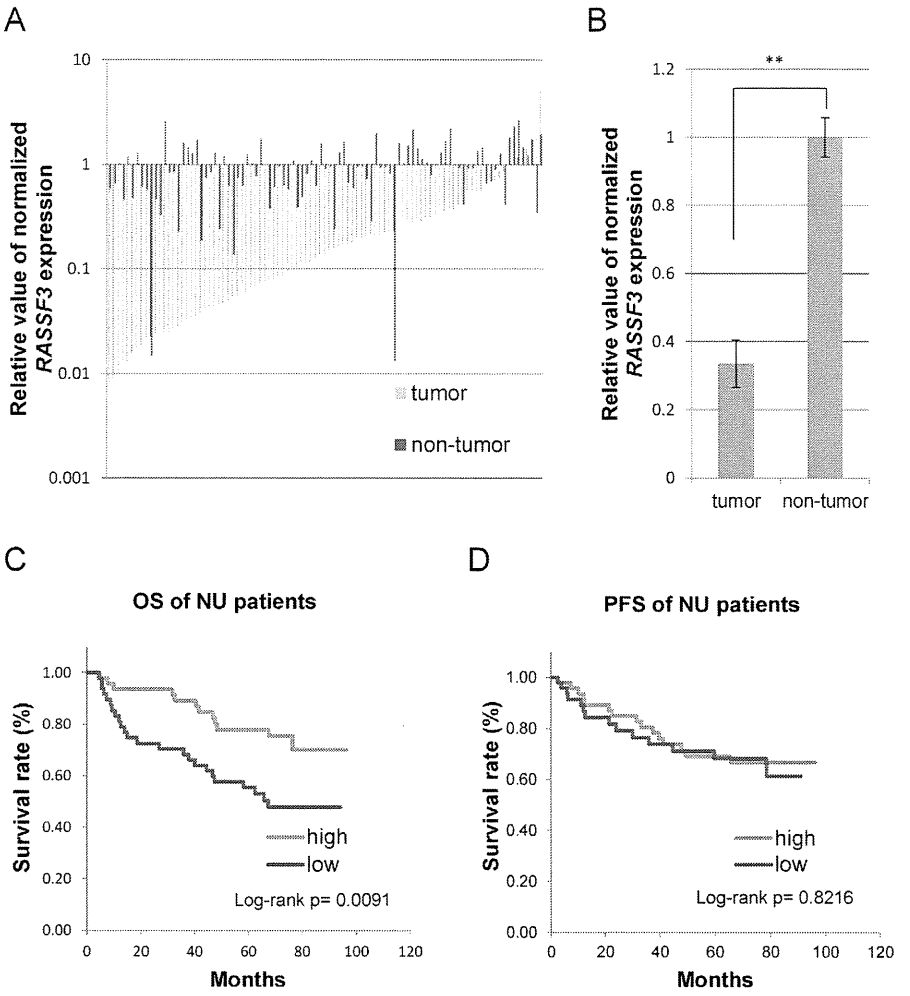

Fig. 1. (A) Relative expression levels of the *RASSF3* gene of NSCLC tumor samples from NU (Nagoya University) hospital and their corresponding non-cancerous lung tissues. Mean of *RASSF3* expression levels of the non-tumor samples was arbitrarily set as 1.0. Expression levels of tumor (blue line) and lung tissue (red line) are indicated side by side from the same patients, with the lowest *RASSF3* level of the tumor starting from the left. (B) Comparison of mean *RASSF3* expression levels between tumor and non-tumor samples. The reduction of *RASSF3* expression in tumor tissues was statistically significant. (C) and (D) Kaplan–Meier analysis of patients for overall survival (OS) (C) and progression-free survival (PFS) (D). The low *RASSF3* expression group showed a significantly worse prognosis in OS but not associated with PFS.

of 95) showed a more significantly reduced level of *RASSF3* (blue line in Fig. 1A) than that in the corresponding normal lung tissue (red line in Fig. 1A), indicating that *RASSF3* is frequently downregulated in NSCLCs. The mean of relative values of normalized *RASSF3* expression was also shown to be significantly lower in tumors than in normal lung tissues (Fig. 1B).

3.2. Low expression of RASSF3 significantly associated with invasive/metastatic character, non-adenocarcinoma histology, and EGFR wild-type status

To determine the possible effects of *RASSF3* downregulation on malignant phenotypes of NSCLCs, we divided 95 cases into two, low ($n=48$) and high ($n=47$) expression groups, respectively, by the median value (=0.14), and conducted statistical analyses for clinicopathological features based on the *RASSF3* expression status. The association status between *RASSF3* expression and clinicopathological parameters is summarized in Table 1. We found that the low *RASSF3* expression group was associated with disease progression in the patients, including TNM stage II/III ($p=0.0011$), tumor size (30 mm<) ($p=0.0123$), lymph node metastasis (pN1<) ($p=0.0008$) and pleural invasion ($p=0.0497$). Low *RASSF3* expression was significantly infrequent in the tumors with *EGFR* mutation ($p=0.0013$). The low *RASSF3* was also less frequently detected in the tumors from female ($p=0.0118$), adenocarcinoma ($p=0.0001$) and never/light smokers ($p=0.0282$), which were known to be the factors related with *EGFR* mutation [17–19]. There was no relation between *RASSF3* expression and *KRAS* mutation ($p=0.6927$).

Next, in order to reveal the crucial parameters for low *RASSF3* expression, we performed logistic regression analysis (Table 2). Univariate logistic regression analysis (Table 2, left column) indicated the same associations as the χ^2 test. In multivariate analysis (Table 2, right column), low *RASSF3* expression was found to be independently associated with non-adenocarcinoma histology, lymph node metastasis, pleural invasion and wild-type *EGFR*.

Among 95 patients, recurrence of the disease was observed in 29 patients, and 36 patients died during follow-up. The median length for OS and PFS of the patients were 71.5 and 65.9 months, respectively (Fig. 1C and D). Statistical analysis revealed that the low *RASSF3* expression group was significantly associated with worse prognosis in OS for the patients ($p=0.0091$, log-rank test) but not in PFS ($p=0.8216$, log-rank test). Since these survival data suggested possible discrepancies, we checked the major causes of death among the 36 patients. Primary lung cancer was the main cause of death in 21, but the remaining 6 patients died of other lung diseases (COPD and pneumonia which did not develop during cancer treatment), 3 of other neoplasms (pancreas cancer and leukemia), one of cerebrovascular accident, one

Table 1
Relationship between clinicopathological features and *RASSF3* gene expression of NSCLC patients from NU.

Variables		*n*	*RASSF3* expression (cutoff = 0.14)		
			Low	High	*p*-Value[a]
Age	≤65	38	19	19	
	>65	57	29	28	0.9332
Sex	Female	29	9	20	
	Male	66	39	27	0.0118*
Smoking history (pack-year)	≤20	36	13	23	
	>20	59	35	24	0.0282*
Histology	Adenocarcinoma	63	23	40	
	Non-adenocarcinoma	32	25	7	0.0001**
	Squamous cell carcinoma	29	23	6	
	Large cell carcinoma	1	0	1	
	Adenosquamous carcinoma	2	2	0	
TNM stage (UICC-7)	Stage I	57	21	36	
	Stage II/III	38	27	11	0.0011**
Tumor size (mm)	≤30	54	21	33	
	>30	40	26	14	0.0123*
Lymph node metastasis	pN0	68	27	41	
	pN1-3	27	21	6	0.0008**
Lymph invasion	–	63	30	33	
	+	32	18	14	0.4265
Venous invasion	–	78	40	38	
	+	16	8	8	0.9255
Pleural invasion	–	51	21	30	
	+	44	27	17	0.0497*
EGFR mutation	Mutant	28	7	21	
	Wild	67	41	26	0.0013**
KRAS mutation	Mutant	6	3	3	
	Wild	89	45	44	0.6927

Values with statistical significance were indicated with * ($p < 0.05$) or ** ($p < 0.01$). NSCLC: non-small cell lung cancer; NU: Nagoya University Hospital; OS: overall survival; PFS: progression-free survival.
[a] χ^2-test.

of renal failure, one of liver cirrhosis and 3 of unknown etiology. Thus, we reanalyzed the disease-specific survival (DSS), and found no significant association with DSS ($p = 0.4527$, log-rank test) (Supplemental Fig. S1). These data suggested that low *RASSF3* expression may not be a sufficient predictor for OS or PFS of NSCLC patients.

3.3. Association of low RASSF3 expression with clinicopathological parameters in the other NSCLC cohort

In order to confirm the results above, we analyzed the other set of NSCLC samples that we collected in Aichi Cancer Center (ACC) Hospital. We again found the frequent downregulation of *RASSF3* in the patients' samples (38 of 45) (Supplementary Fig. S2A). Like the NU sample set, we divided the 45 cases into two groups by median value (=0.35) as the low- ($n = 22$) and high-expression groups ($n = 23$) and compared these two groups. As we observed in NU samples, similar associations of *RASSF3* expression with disease progression and *EGFR* mutation were detected in ACC samples (Supplementary Table 3). Although there was no significant difference in tumor size in this cohort, we confirmed that the advanced TNM stage and lymph node metastasis were significantly associated with low *RASSF3* expression. No relation between *RASSF3* expression and *KRAS* mutation or *TP53* mutation was also found. In multivariate logistic regression analysis, we found similar tendencies between low *RASSF3* expression and clinicopathological parameters such as non-adenocarcinoma histology and lymph node metastasis (Supplementary Table 4). However, we did not detect any independent statistical significance, which was probably due to the smaller cohort sample.

Among 45 patients, 10 died during follow-up, with the OS median length of 95.5 months (Supplementary Fig. S2B). *RASSF3* expression levels were not significantly associated with OS ($p = 0.4270$, log-rank test).

Table 2
Univariate and multivariate logistic regression analyses of the association between low *RASSF3* gene expression and clinicopathological features of NU patients.

Variables	Univariate				Multivariate			
	Odds ratio	95% CI		*p*-Value[a]	Odds ratio	95% CI		*p*-Value[a]
Age (>65)	1.0357	0.4557	2.3539	0.9332				
Sex (male)	3.2099	1.2700	8.1126	0.0137*				
Smoking history (>20 pack-years)	2.5801	1.0964	6.0715	0.0299*				
Histology (non-adenocarcinoma)	6.2112	2.3251	16.5924	0.0003**	4.2469	1.4132	12.7629	0.0100**
TNM Stage (UICC-7) (II/III)	4.2078	1.7387	10.1834	0.0014**				
Size (>30 mm)	2.9184	1.2481	6.8238	0.0135*				
Lymph node metastasis (pN1-3)	5.3148	1.8990	14.8744	0.0015**	5.2127	1.6251	16.7206	0.0055**
Lymph invasion	1.4143	0.6010	3.3279	0.4272				
Venous invasion	0.9500	0.3240	2.7859	0.9256				
Pleural invasion	2.2689	0.9952	5.1730	0.0514	2.7348	1.0001	7.4786	0.0500*
EGFR mutation	0.2114	0.0788	0.5669	0.0020**	0.2214	0.0671	0.7309	0.0133*
KRAS mutation	0.9778	0.1871	5.1085	0.9787				

Values with statistical significance were indicated with *($p < 0.05$) or **($p < 0.01$). NU: Nagoya University Hospital; CI: confidence interval.
[a] Logistic regression analysis.

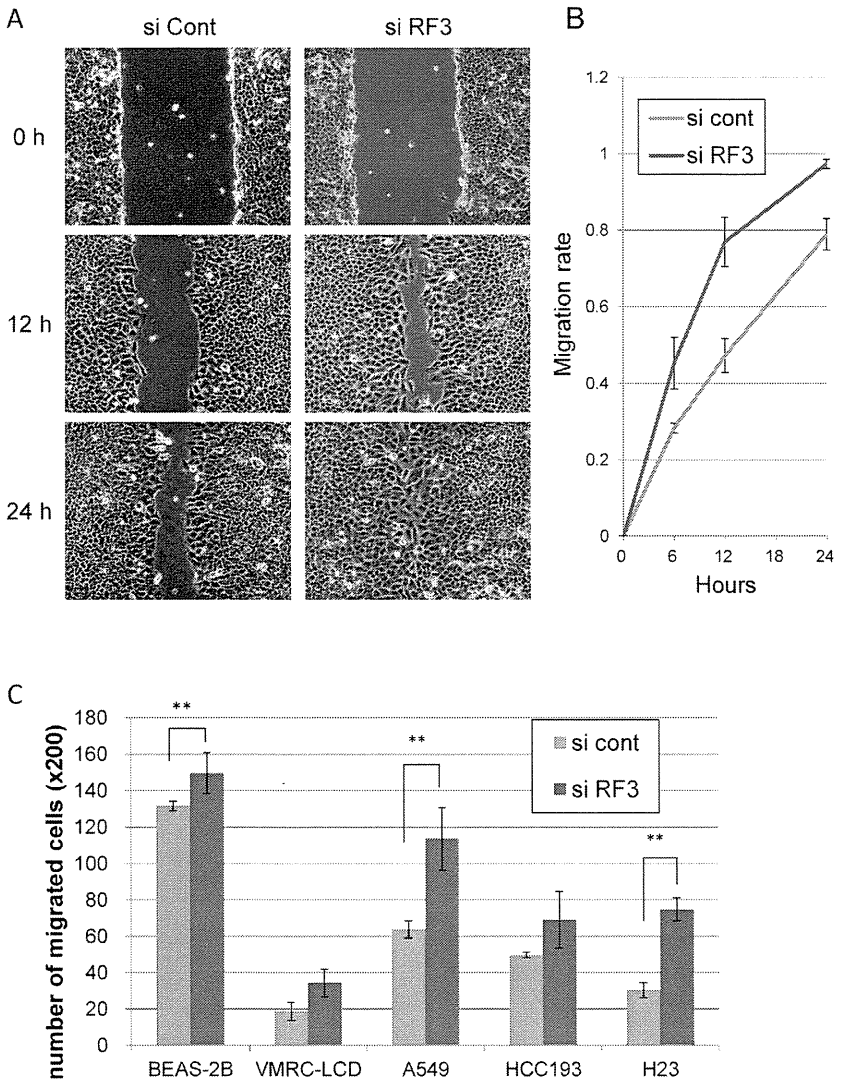

Fig. 2. RASSF3 knockdown enhances cell motility in the wound healing assay (A and B) and transwell migration assay (C). (A) Forty-eight hours after the transfection, A549 cells were re-plated in 3.5 cm dishes. After the cells had grown to confluence, cultures were damaged using 1–200 μl beveled orifice tip and then allowed to migrate. Photographs were taken at the indicated time points. (B) Migration rate is designated as a – b/a (a and b represent the widths of the fissures at time 0 and each time point, respectively). RASSF3-knockdown cells increased migration rate compared to the control. (C) Transwell migration assay. Cell lines transfected with siRNA were re-plated into a transwell chamber 48 h after the transfection and cells were counted after 24 h incubation. RASSF3-knockdown statistically significantly enhanced migration ability of 3 cell lines (A549, BEAS-2B, and NCI-H23). Although HCC193 also showed enhancement by RASSF3-knockdown, it was not statistically significant. The migration ability of VMRC-LCD was exceptionally low, and hardly affected by RASSF3-knockdown. si RF3: siRNA against RASSF3; si Cont: negative control siRNA.

3.4. DNA hypermethylation not a main cause of RASSF3 downregulation

In order to determine whether or not low *RASSF3* expression was induced by DNA hypermethylation, we studied the DNA methylation status at the CpG island of the *RASSF3* gene promoter region using lung cancer cell lines. Fourteen lung cancer cell lines showed various *RASSF3* expression levels compared with an immortalized normal bronchial epithelial cell line BEAS-2B, the majority of which showed lower expression than in BEAS-2B (Supplemental Fig. 3A). However, we detected no CpG island methylation in the promoter region of the *RASSF3* gene in 14 lung cancer cell lines (Supplemental Fig. 3B). We also examined 8 NSCLC clinical samples from the low *RASSF3* expression group. However, we could not find DNA methylation in any specimens. These results suggested that DNA hypermethylation was not a major cause of *RASSF3* downregulation (Supplemental Fig. 3C).

3.5. Silence of RASSF3 increases migration rate in NSCLC cells

The above results suggested that RASSF3 downregulation was associated with more malignant phenotypes including lymph node metastasis. To determine whether RASSF3 suppression promotes lung cancer cell migration ability in vitro, we transfected either RASSF3 targeted or control siRNA into four lung cancer cell lines (A549, HCC193, NCI-H23, and VMRC-LCD) and one immortalized bronchial epithelial cell line (BEAS-2B), and conducted wound healing and transwell migration assays. In the wound healing assay, migration ability was increased in RASSF3-knockdown A549 cells compared to the control cells (Fig. 2A and B). Similar results were obtained with three other cell lines including BEAS-2B, NCI-H23, and HCC193 (Supplemental Fig. S4). Similarly, in the transwell migration assay, RASSF3-knockdown enhanced migration ability of those 4 cell lines (A549, HCC193, NCI-H23, and BEAS-2B), although the enhancement in HCC193 was not statistically significant (Fig. 2C

and Supplemental Fig. S5). Because the migration ability of VMRC-LCD was exceptionally low, the effect of RASSF3-knockdown can be hardly evaluated in this cell line (Fig. 2C, Supplemental Figs. S4D, S4H, and S5).

4. Discussion

In the present study, we demonstrated that *RASSF3* expression was frequently downregulated in NSCLCs. Decrease of its expression was significantly associated with the progressive phenotypes of lung cancer including lymph node metastasis and pleural invasion. The strong correlation of lower *RASSF3* expression with such malignant phenotypes may imply that *RASSF3* downregulation plays an important role in cancer cell migration or invasion. This idea is supported by our in vitro studies which showed that RASSF3 knockdown promoted cell migration abilities of lung cancer cell lines. In this regard, we previously reported that RASSF3 stabilized p53 [16], and p53 was also shown to negatively regulate epithelial to mesenchymal transition (EMT) induced by TGF-β [20]. One possible mechanism of the tumor suppressive activity of RASSF3 might be a negative control of EMT through p53 stabilization. In this regard, EMT induction has been indicated to account for increased cancer cell migration/invasion [21]. However, although our preliminary in vitro experiments were suggestive, they failed to provide sufficient evidence to confirm EMT induction in the lung cancer cells by RASSF3-knockdown (data not shown).

The low *RASSF3* expression group also showed a correlation with wild-type *EGFR* status in univariate analysis. Multivariate analysis also revealed this correlation between RASSF3 and EGFR, indicating that this relationship was independent from other parameters. These data might suggest that the signaling pathways were regulated by RASSF3 and EGFR crosstalk in-between, and thus the alteration or mutation of each gene is mutually exclusive. On this point, Cui et al. reported that desmocollin 3, the target gene of p53, inhibits the EGFR/ERK pathway in human lung cancer [22]. Since RASSF3 stabilizes p53 [16], RASSF3 silencing might downregulate desmocollin 3 expression through p53 destabilization, resulting in activation of the EGFR/ERK pathway. However, further studies are needed to clarify whether or not such an interaction between the EGFR and RASSF3 signaling exists.

We found no significant correlation between *RASSF3* expression and patients' survival. This seemed to contradict the significant correlation of *RASSF3* with lymph node metastasis or pleural invasion in this study, where both were strong predictors of poor prognosis [23–25]. In this regard, previous studies reported that postoperative therapy has a strong influence on patients' survival, which we had earlier suspected to explain this inconsistency [26,27]. However, we found no remarkable difference in postoperative treatment between the two expression groups. Although we conducted further subset analyses of various kinds to explain this discrepancy, no significant factors were identified.

Finally, to determine the underlying mechanisms of *RASSF3* downregulation, we examined 14 lung cancer cell lines and 8 lung tumor specimens from the low expression group. However, we found no methylation of CpGs in the *RASSF3* promoter region. Previous studies also reported no methylation of *RASSF3* in 8 colorectal cancer cell lines, 8 thyroid cancer cell lines or 6 glioma cell lines [28–30]. Thus, simple hypermethylation of the promoter region may not be the primary mechanism to suppress RASSF3 transcription.

In conclusion, the present study showed that RASSF3 is frequently downregulated in NSCLCs, leading to an increase in lymph node metastasis or pleural invasion. These results indicate that RASSF3 is a tumor suppressor of lung cancer. Furthermore, the possible interaction between the RASSF3 and EGFR signaling might give new clues to dissect the complicated pathogenesis of lung cancer, which has long been virtually insurmountable riddle.

Conflict of interest statement

None declared.

Acknowledgments

This work was supported in part by JSPS KAKENHI (22300338, 2465065 YS, 23790725 KN, 22590267 YH), and a Grant-in-Aid for Third-Term Comprehensive Control Research for Cancer from the Ministry of Health, Labor and Welfare of Japan, and the Takeda Science Foundation (YS, KN). We thank Ms. Miwako Nishizawa for her excellent technical assistance.

Appendix A. Supplementary data

Supplementary data associated with this article can be found, in the online version, at http://dx.doi.org/10.1016/j.lungcan.2013.10.014.

References

[1] Jemal A, Bray F, Center MM, Ferlay J, Ward E, Forman D. Global cancer statistics. CA Cancer J Clin 2011;61:69–90.
[2] Richter AM, Pfeifer GP, Dammann RH. The RASSF proteins in cancer; from epigenetic silencing to functional characterization. Biochim Biophys Acta 2009;1796:114–28.
[3] Pfeifer GP, Dammann R, Tommasi S. RASSF proteins. Curr Biol 2010;20:R344–5.
[4] Sherwood V, Recino A, Jeffries A, Ward A, Chalmers AD. The N-terminal RASSF family: a new group of Ras-association-domain-containing proteins, with emerging links to cancer formation. Biochem J 2010;425:303–11.
[5] Underhill-Day N, Hill V, Latif F. N-terminal RASSF family: RASSF7-RASSF10. Epigenetics 2011;6:284–92.
[6] Dammann R, Li C, Yoon JH, Chin PL, Bates S, Pfeifer GP. Epigenetic inactivation of a RAS association domain family protein from the lung tumour suppressor locus 3p21.3. Nat Genet 2000;25:315–9.
[7] Burbee DG, Forgacs E, Zochbauer-Muller S, Shivakumar L, Fong K, Gao B, et al. Epigenetic inactivation of RASSF1A in lung and breast cancers and malignant phenotype suppression. J Natl Cancer Inst 2001;93:691–9.
[8] Endoh H, Yatabe Y, Shimizu S, Tajima K, Kuwano H, Takahashi T, et al. RASSF1A gene inactivation in non-small cell lung cancer and its clinical implication. Int J Cancer 2003;106:45–51.
[9] Ito M, Ito G, Kondo M, Uchiyama M, Fukui T, Mori S, et al. Frequent inactivation of RASSF1A, BLU, and SEMA3B on 3p21.3 by promoter hypermethylation and allele loss in non-small cell lung cancer. Cancer Lett 2005;225:131–9.
[10] Wang J, Wang B, Chen X, Bi J. The prognostic value of RASSF1A promoter hypermethylation in non-small cell lung carcinoma: a systematic review and meta-analysis. Carcinogenesis 2011;32:411–6.
[11] Jo H, Kim JW, Kang GH, Park NH, Song YS, Kang SB, et al. Association of promoter hypermethylation of the RASSF1A gene with prognostic parameters in endometrial cancer. Oncol Res 2006;16:205–9.
[12] Ma L, Zhang JH, Liu FR, Zhang X. Hypermethylation of promoter region of RASSF1A gene in ovarian malignant epithelial tumors. Zhonghua Zhong Liu Za Zhi 2005;27:657–9.
[13] Sugawara W, Haruta M, Sasaki F, Watanabe N, Tsunematsu Y, Kikuta A, et al. Promoter hypermethylation of the RASSF1A gene predicts the poor outcome of patients with hepatoblastoma. Pediatr Blood Cancer 2007;49:240–9.
[14] Tommasi S, Dammann R, Jin SG, Zhang XF, Avruch J, Pfeifer GP. RASSF3 and NORE1: identification and cloning of two human homologues of the putative tumor suppressor gene RASSF1. Oncogene 2002;21:2713–20.
[15] Jacquemart IC, Springs AE, Chen WY. Rassf3 is responsible in part for resistance to mammary tumor development in neu transgenic mice. Int J Oncol 2009;34:517–28.
[16] Kudo T, Ikeda M, Nishikawa M, Yang Z, Ohno K, Nakagawa K, et al. The RASSF3 candidate tumor suppressor induces apoptosis and G1-S cell-cycle arrest via p53. Cancer Res 2012;72:2901–11.
[17] Paez JG, Janne PA, Lee JC, Tracy S, Greulich H, Gabriel S, et al. EGFR mutations in lung cancer: correlation with clinical response to gefitinib therapy. Science 2004;304:1497–500.
[18] Pao W, Miller V, Zakowski M, Doherty J, Politi K, Sarkaria I, et al. EGF receptor gene mutations are common in lung cancers from never smokers and are associated with sensitivity of tumors to gefitinib and erlotinib. Proc Natl Acad Sci U S A 2004;101:13306–11.
[19] Shigematsu H, Lin L, Takahashi T, Nomura M, Suzuki M, Wistuba II, et al. Clinical and biological features associated with epidermal growth factor receptor gene mutations in lung cancers. J Natl Cancer Inst 2005;97:339–46.

[20] Termen S, Tan EJ, Heldin CH, Moustakas A. p53 regulates epithelial-mesenchymal transition induced by transforming growth factor beta. J Cell Physiol 2013;228:801–13.
[21] Thomson S, Petti F, Sujka-Kwok I, Mercado P, Bean J, Monaghan M, et al. A systems view of epithelial-mesenchymal transition signaling states. Clin Exp Metastasis 2011;28:137–55.
[22] Cui T, Chen Y, Yang L, Knosel T, Huber O, Pacyna-Gengelbach M, et al. The p53 target gene desmocollin 3 acts as a novel tumor suppressor through inhibiting EGFR/ERK pathway in human lung cancer. Carcinogenesis 2012;33:2326–33.
[23] Fukui T, Mori S, Yokoi K, Mitsudomi T. Significance of the number of positive lymph nodes in resected non-small cell lung cancer. J Thorac Oncol 2006;1:120–5.
[24] Shimizu K, Yoshida J, Nagai K, Nishimura M, Ishii G, Morishita Y, et al. Visceral pleural invasion is an invasive and aggressive indicator of non-small cell lung cancer. J Thorac Cardiovasc Surg 2005;130:160–5.
[25] Kanzaki R, Ikeda N, Okura E, Kitahara N, Shintani Y, Okimura A, et al. Surgical results and staging of non-small cell lung cancer with interlobar pleural invasion. Interact Cardiovasc Thorac Surg 2012;14:739–42.
[26] Heon S, Johnson BE. Adjuvant chemotherapy for surgically resected non-small cell lung cancer. J Thorac Cardiovasc Surg 2012;144:S39–42.
[27] Tsuboi M, Ohira T, Saji H, Miyajima K, Kajiwara N, Uchida O, et al. The present status of postoperative adjuvant chemotherapy for completely resected non-small cell lung cancer. Ann Thorac Cardiovasc Surg 2007;13:73–7.
[28] Hesson LB, Wilson R, Morton D, Adams C, Walker M, Maher ER, et al. CpG island promoter hypermethylation of a novel Ras-effector gene RASSF2A is an early event in colon carcinogenesis and correlates inversely with K-ras mutations. Oncogene 2005;24:3987–94.
[29] Schagdarsurengin U, Richter AM, Hornung J, Lange C, Steinmann K, Dammann RH. Frequent epigenetic inactivation of RASSF2 in thyroid cancer and functional consequences. Mol Cancer 2010;9:264.
[30] Hesson L, Bieche I, Krex D, Criniere E, Hoang-Xuan K, Maher ER, et al. Frequent epigenetic inactivation of RASSF1A and BLU genes located within the critical 3p21.3 region in gliomas. Oncogene 2004;23:2408–19.

Gastroenterology 2014;146:562–572

Hepatitis Virus Infection Affects DNA Methylation in Mice With Humanized Livers

Yasuyuki Okamoto,[1,2,3,*] Keiko Shinjo,[1,4,*] Yasuhiro Shimizu,[5] Tsuyoshi Sano,[5] Kenji Yamao,[6] Wentao Gao,[7] Makiko Fujii,[2] Hirotaka Osada,[2] Yoshitaka Sekido,[2] Shuko Murakami,[8] Yasuhito Tanaka,[8] Takashi Joh,[3] Shinya Sato,[9] Satoru Takahashi,[9] Takaji Wakita,[10] Jingde Zhu,[11] Jean-Pierre J. Issa,[12] and Yutaka Kondo[1,2,13]

[1]Division of Epigenomics and [2]Division of Molecular Oncology, Aichi Cancer Center, Nagoya, Japan; [3]Department of Gastroenterology and Metabolism, Nagoya City University Graduate School of Medicine, Nagoya, Japan; [4]Division of Oncological Pathology, [5]Department of Gastroenterological Surgery, and [6]Department of Gastroenterology, Aichi Cancer Center, Nagoya, Japan; [7]Department of General Surgery, the First Affiliated Hospital of Nanjing Medical University, Nanjing, China; [8]Department of Virology and Liver Unit and [9]Department of Experimental Pathology and Tumor Biology, Nagoya City University Graduate School of Medical Sciences, Nagoya, Japan; [10]Department of Virology II, National Institute of Infectious Diseases, Tokyo, Japan; [11]Cancer Epigenetics Program, Shanghai Cancer Institute, Shanghai Jiaotong University, Shanghai, China; [12]Fels Institute for Cancer Research and Molecular Biology, Temple University School of Medicine, Philadelphia, Pennsylvania; and [13]Precursory Research for Embryonic Science and Technology, Japan Science and Technology Agency, Saitama, Japan

BACKGROUND & AIMS: Cells of tumors associated with chronic inflammation frequently have altered patterns of DNA methylation, including hepatocellular carcinomas. Chronic hepatitis has also been associated with aberrant DNA methylation, but little is known about their relationship. **METHODS:** Pyrosequencing was used to determine the methylation status of cultured Huh7.5.1 hepatoma cells after hepatitis C virus (HCV) infection. We also studied mice with severe combined immunodeficiency carrying the urokinase-type plasminogen activator transgene controlled by an albumin promoter (urokinase-type plasminogen activator/severe combined immunodeficient mice), in which up to 85% of hepatocytes were replaced by human hepatocytes (chimeric mice). Mice were given intravenous injections of hepatitis B virus (HBV) or HCV, liver tissues were collected, and DNA methylation profiles were determined at different time points after infection. We also compared methylation patterns between paired samples of hepatocellular carcinomas and adjacent nontumor liver tissues from patients. **RESULTS:** No reproducible changes in DNA methylation were observed after infection of Huh7.5.1 cells with HCV. Livers from HBV- and HCV-infected mice had genome-wide, time-dependent changes in DNA methylation, compared with uninfected urokinase-type plasminogen activator/severe combined immunodeficient mice. There were changes in 160 ± 63 genes in HBV-infected and 237 ± 110 genes in HCV-infected mice. Methylation of 149 common genes increased in HBV- and HCV-infected mice; methylation of some of these genes also increased in hepatocellular carcinoma samples from patients compared with nontumor tissues. Expression of *Ifng*, which is expressed by natural killer cells, increased significantly in chimeric livers, in concordance with induction of DNA methylation, after infection with HBV or HCV. Induction of *Ifng* was reduced after administration of an inhibitor of natural killer cell function (anti–asialo GM1). **CONCLUSIONS:** In chimeric mice with humanized livers, infection with HBV and HCV appears to activate a natural kill cell–dependent innate immune response. This contributes to the induction and accumulation of aberrant DNA methylation in human hepatocytes.

Keywords: Epigenetic; Inflammatory Response; Liver Cancer; Gene Regulation.

BASIC AND TRANSLATIONAL LIVER

The majority of hepatocellular carcinomas (HCCs) occur as a consequence of chronic hepatitis and liver cirrhosis, particularly after infection with hepatitis B virus (HBV) or hepatitis C virus (HCV).[1] Aberrant DNA methylation in the promoter CpG islands has been described in many types of human cancers, including HCCs. This epigenetic alteration, sometimes together with point mutations and deletions, serves as a mechanism that leads to inactivation of cancer-related genes connected with essential tumor properties, such as tumor cell proliferation, anti-apoptosis, neoangiogenesis, and chemotherapy resistance.[2,3]

In earlier studies, we and other groups demonstrated that aberrant DNA methylation was detected even in precancerous liver tissues, such as chronic hepatitis, liver cirrhosis, or dysplastic nodules, suggesting that DNA methylation is an early and ubiquitous event during HCC development.[4–8] Intriguingly, these studies consistently showed that certain

*Authors share co-first authorship.

Abbreviations used in this paper: ESR1, estrogen receptor 1; HBV, hepatitis B virus; HBx, hepatitis B virus X; HCC, hepatocellular carcinoma; HCV, hepatitis C virus; HOXA6, homeobox A6; IFN, interferon; MCAM, methylated CpG island amplification microarray; NK, natural killer; PCNA, proliferating cell nuclear antigen; RASSF1A, Ras association domain family 1 isoform A; ROS, reactive oxygen species; SCID, severe combined immunodeficient.

0016-5085/$36.00
http://dx.doi.org/10.1053/j.gastro.2013.10.056

genes, such as the tumor suppressor Ras association domain family 1 isoform A (*RASSF1A*), are frequently methylated in precancerous tissues as well as cancerous tissues, regardless of the type of hepatitis virus infection. This suggests that DNA methylation of certain genes might reflect the clinical course of persistent inflammation, and a subset of cells that have acquired aberrant DNA methylation in their promoters could be prone to cancer formation.

Regarding the cause of aberrant DNA methylation, a connection between chronic inflammation and DNA methylation has been suggested for a long time, however, the key factors linking these 2 processes are not completely understood. Several studies have shown that hepatitis B virus X protein, as well as HCV protein, could induce regional hypermethylation of specific tumor suppressor genes.[9–12] These findings indicate the role of the hepatitis B virus X protein and HCV protein as important players in hepatitis virus–induced epigenetic aberrations. However, a previous genome-wide DNA methylation analysis revealed that CpG island promoters were methylated in different patterns during progression of the disease, suggesting that multiple mechanisms were involved in the acquisition of epigenetic changes during the development of HCCs.[8]

Recent technological advances have enabled the development of severe combined immunodeficient (SCID) mouse carrying a urokinase-type plasminogen activator transgene controlled by an albumin promoter (urokinase-type plasminogen activator/SCID mouse), in which the liver is repopulated with human hepatocytes (human hepatocyte chimeric mouse).[13,14] This mouse model shows severe combined immunodeficiency due to lack of both T- and B-cell activities, but possesses normal macrophages and natural killer (NK) cell activity, which are important components of the innate immune system. Because both HBV and HCV can infect human hepatocytes, but not murine hepatocytes, this model is a useful tool for mimicking and unraveling hepatitis virus–host interactions in vivo.[14–16] Using this model, we demonstrated here that DNA methylation was induced in human hepatocytes after HBV and HCV infections, and that induction of DNA methylation was closely associated with NK cell activity.

Materials and Methods

Tissue Samples

Paired samples of adjacent noncancerous liver tissue and cancerous tissue were obtained from 34 patients with HCC who underwent surgical resection at the Aichi Cancer Center Hospital in accordance with institutional policies (Supplementary Table 1, Supplementary Methods). All patients provided written informed consent. In addition, samples of normal liver tissue were also obtained from 8 patients without HBV or HCV infection who underwent partial hepatectomy for liver metastasis of primary colon cancer.

Cell Lines and Culture Conditions

The hepatoma cell line, Huh7.5.1 (a gift from Dr Francis V. Chisari), was grown in Dulbecco's modified Eagle medium (Invitrogen, Carlsbad, CA) with 10% fetal bovine serum in plastic tissue culture plates in a humidified atmosphere containing 5% CO_2 at 37°C. An efficient tissue culture-based HCV infection system in Huh7.5.1 cells was conducted using the HCV-JFH1 strain.[17] Infection of HCV-JFH1 was confirmed by reverse transcription polymerase chain reaction at 7, 9, 10, 21, and 26 weeks after initial infection (Supplementary Figure 1).

Establishment of HBV or HCV Infection in Human Hepatocyte Chimeric Mouse

The chimeric mice, in which up to 85% of hepatocytes in the liver were repopulated by human hepatocytes, were obtained from Phoenix Bio Co, Ltd (Hiroshima, Japan). Human hepatocytes were derived from 7 different individuals (2 to 28 years old, 3 females and 4 males). No significant difference in basal level of DNA methylation was observed between the transplanted hepatocytes of each mouse. Forty-seven chimeric mice were intravenously injected with either HBV or HCV (1.0×10^4 copies, respectively) and successfully infected (HBV, 23 mice; HCV, 24 mice; Supplementary Table 2). In order to inhibit the mouse NK cell activity, 10 chimeric mice were treated with 20 μL (0.02 mg/body) anti–asialo GM1 (#986-10001; Wako Pure Chemical Industries, Osaka, Japan) 2 times per week from 1 day before the hepatitis virus infection until they were sacrificed. Two mice were treated with the nonspecific rabbit polyclonal antibody (#AB-105-C; R&D Systems, Minneapolis, MN) as a control for the anti–asialo GM1 treatment. Because the levels of cytokines, reactive oxygen species (ROS) induction, and cell proliferation in these 2 control mice were concordant with those in mice without nonspecific rabbit polyclonal antibody treatment, we combined the data of mice with and without treatment of nonspecific rabbit polyclonal antibody for use as control data. Five chimeric mice were treated with 0.2 mg of anti-mouse interferon (IFN)-gamma–neutralizing rat monoclonal antibody (Clone XMG1.2, 40-7311; TONBO, San Diego, CA) 2 times per week from 1 day before hepatitis virus infection.[18] In order to evaluate hepatocyte proliferation, bromodeoxyuridine (550891; BD, Franklin Lakes, NJ) was injected 2 hours before the sacrifice (Supplementary Table 2).

Bisulfite-Pyrosequencing for DNA Methylation Analysis

DNA methylation levels were measured by pyrosequencing technology using species-specific primer sets, which can discriminately amplify either mouse genes or human genes (Supplementary Table 3, Supplementary Methods).

Methylated CpG Island Amplification-Microarray

Methylated CpG island amplification-microarray (MCAM) was carried out to analyze the methylation status of 34 cancerous tissues from HCC patients, Huh7.5.1 cells infected with HCV-JFH1, and samples from 20 human hepatocyte chimeric mice (Supplementary Figure 2, Supplementary Methods). A detailed protocol of MCAM is described in the Supplementary Methods.

Measurement of ROS Production

ROS production was evaluated by staining with dihydroethidium (Invitrogen).[16] In the presence of ROS, dihydroethidium is oxidized to ethidium bromide that stains nuclei bright red by means of intercalation into DNA. Intracellular ROS level of Huh7.5.1 was evaluated using an ROS/reactive nitrogen species detection kit (Enzo Life Sciences, Plymouth Meeting, PA) according to manufacturer's protocol. The fluorescent signals were analyzed using an AF7000 fluorescent microscope (Leica Microsystems, Wetzlar, Germany).

Statistical Analysis

All statistical analyses were performed using JMP statistical software version 10. Fisher's exact test was used to determine nonrandom associations between 2 categorical variables.

Kruskal-Wallis analysis was used to evaluate the extent of differences among more than 3 groups. All reported P values are 2-sided, with $P < .05$ considered statistically significant.

Results

DNA Methylation Analysis in HCC Samples

We initially assessed the genome-wide DNA methylation status in clinical HCCs. MCAM was performed in 34 HCC samples (Supplementary Table 1). DNA methylation was most frequently observed in cancerous tissues from the patients with liver cirrhosis background and HCV infection in comparison with the other types of histological or viral status (mean 599 ± 131 genes; $P = .0034$; Figure 1*A* and *B*). These data indicated that a long period of chronic HCV infection was closely associated with accumulation of aberrant DNA methylation, as reported previously.[4,8,19]

Among the frequent methylation target genes, which were methylated in >25% of the cases in each group, many genes were commonly methylated in both HBV-associated (85 of 212 genes [40%]) and HCV-associated (85 of 289 genes [29%]) adjacent noncancerous tissues (Figure 1*C*). This was more obvious in cancerous tissues; 338 genes were commonly methylated in HBV-associated (407 genes [83%]) and HCV-associated (657 genes [51%]) HCCs. The majority of the methylated genes in HBV-associated cancerous tissues were also methylated in HCV-associated cancerous tissues, and HCV-associated cancerous tissues had a number of specifically methylated genes (319 of 657 genes [49%]). These data suggest that there is a common mechanism for the induction of aberrant DNA methylation between HBV and HCV infection and that HCV might play a role in accelerating the methylation process.[19]

HCV Infection In Vitro Did Not Induce Aberrant DNA Methylation in a Hepatocellular Carcinoma Cell Line

The clinical data argued that HCV infection can enhance the induction of DNA methylation in hepatocytes. To address this possibility, we evaluated for DNA methylation using a tissue culture–based HCV-infection system. HCV-JFH1 clone was used to infect a Huh-7–derived cell line (Huh7.5.1) that allowed the production and efficient propagation of virus in tissue culture.[20] First, we assessed for genome-wide DNA methylation status and found no reproducible gain of DNA methylation in the HCV-infected Huh7.5.1 cells in comparison with the uninfected cells (Figure 1*D*). Consistently, quantitative DNA methylation analysis revealed that no significant difference in the DNA methylation level of *LINE1*, which represents overall methylation status,[21] was observed between HCV-infected Huh7.5.1 cells and the uninfected cells at 26 weeks (Figure 1*E*, Supplementary Table 5). The methylation level of the GRAM domain containing 3 gene, which is frequently methylated in clinical HCC samples, but not in uninfected Huh7.5.1 cells, remained unmethylated in the HCV-infected Huh7.5.1 cells at 26 weeks (Figure 1*E*). Notably, in vitro HCV infection did not enhance the proliferation of Huh7.5.1 and moderately increased ROS production (Supplementary Figure 5). Our findings demonstrated that HCV infection itself did not induce DNA methylation in this in vitro HCV infection system.

DNA Methylation Analysis in Human Hepatocyte Chimeric Mice With HBV or HCV Infection

In order to unravel the effects of virus–host interactions, especially their impact on DNA methylation in vivo, we examined DNA methylation status in human hepatocyte chimeric mice after infection with HBV (HBV mice) or HCV (HCV mice) (Supplementary Table 2). Both HBV mice (n = 10) and HCV mice (n = 10) were sacrificed at different time points and analyzed for genome-wide DNA methylation status using MCAM. The number of methylated genes in HCV mice was similar to or slightly more than that in HBV mice (Figure 2*A*, mean 237 ± 110 genes vs 160 ± 63 genes, respectively; Supplementary Table 4). More genes were methylated in long-term HBV- or HCV-infected mice (≥16 weeks) than in short to middle-term infected mice (<16 weeks), suggesting that aberrant DNA methylation propagated in a time-dependent manner after viral infection (Figure 2*A*).

The majority of methylated genes in HBV mice were also methylated in HCV mice (149 of 214 genes [70%]), and about half of the methylated genes in HCV mice were specific to these mice (146 of 295 genes [50%]; Figure 2*B*). These data obtained in the mouse model were consistent with the clinical data of HCCs (Figure 1*C*). In addition, a number of methylated genes in human clinical samples were also methylated in HBV mice (Figure 2*C*; 78 of 214 genes [36%]) and HCV mice (134 of 295 genes [45%]). The human hepatocyte chimeric mouse with either HBV or HCV infection appeared to represent the virus–host interactions in human liver and can be an appropriate model to study the mechanisms of induction of aberrant DNA methylation by viral infection in vivo.

Time-Dependent Alterations in DNA Methylation After HBV and HCV Infections

We then evaluated the precise changes in DNA methylation at different time points after viral infection by

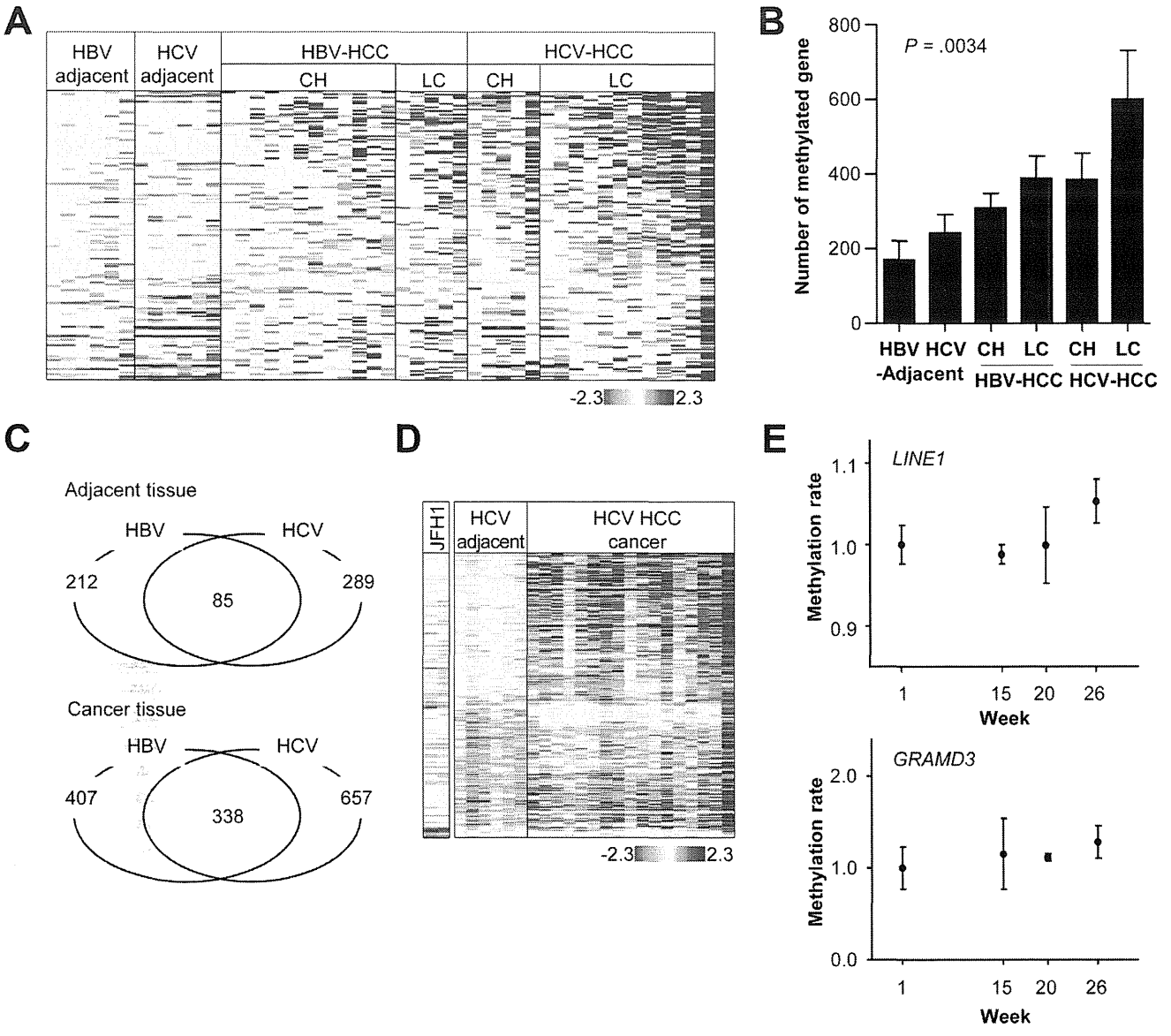

Figure 1. DNA methylation analysis in HCCs. (*A*) Heatmap overview of 940 significantly methylated genes in cancerous tissues (17 cases each of samples associated with HBV and HCV infections) from chronic hepatitis (CH) patients and liver cirrhosis (LC) patients, and corresponding adjacent noncancerous tissues (6 cases each of samples associated with HBV and HCV infections). *Red* and *blue* in cells reflect high and low methylation levels, respectively, as indicated in the scale bar (log2-transformed scale). (*B*) Mean number of hypermethylated genes in clinical samples. Kruskal-Wallis analysis was used to evaluate the extent of differences among the groups ($P = .0034$). (*C*) Number of DNA methylation target genes in HBV-associated and HCV-associated HCCs are shown by Venn diagram (*upper panel*, adjacent noncancerous tissues; *lower panel*, cancerous tissues). (*D*) Heatmap overview of 880 methylated genes in Huh7.5.1 cells infected with HCV-JFH1 (at 26 weeks after infection, duplicated results), and 6 adjacent noncancerous and 17 cancerous tissues from HCV-HCC patients. (*E*) DNA methylation levels of *LINE1* and GRAM domain containing 3 in Huh7.5.1 cells after HCV-JFH1 infection at 1 week, 15 weeks, 20 weeks, and 26 weeks after infection. Y-axis indicates relative values of DNA methylation level in HCV-JFH1–infected Huh7.5.1 to that of uninfected Huh7.5.1 cells. GRAMD3, GRAM domain containing 3.

pyrosequencing analysis in 16 HBV mice and 16 HCV mice (Supplementary Table 2). Methylation of the *LINE1* gene as an indicator of global methylation status has been shown to be inversely associated with tumor transformation.[3,21] The level of *LINE1* methylation in long-term HCV-infected mice was significantly lower than in uninfected control mice (Figure 3*A*; $P = .037$). A similar tendency was also observed in long-term HBV-infected mice, although the decreased methylation level was not statistically significant. Next, 5 genes were selected from the list of MCAM data. Estrogen receptor 1 (*ESR1*) and homeobox A6 (*HOXA6*) were the most frequently methylated in both clinical samples and the mouse models as assessed by MCAM analysis. Zinc finger protein 385A and ELOVL fatty acid elongase 3 genes were less frequently methylated as compared with *ESR1* and *HOXA6* in MCAM analysis. *RASSF1A* is a well-known tumor

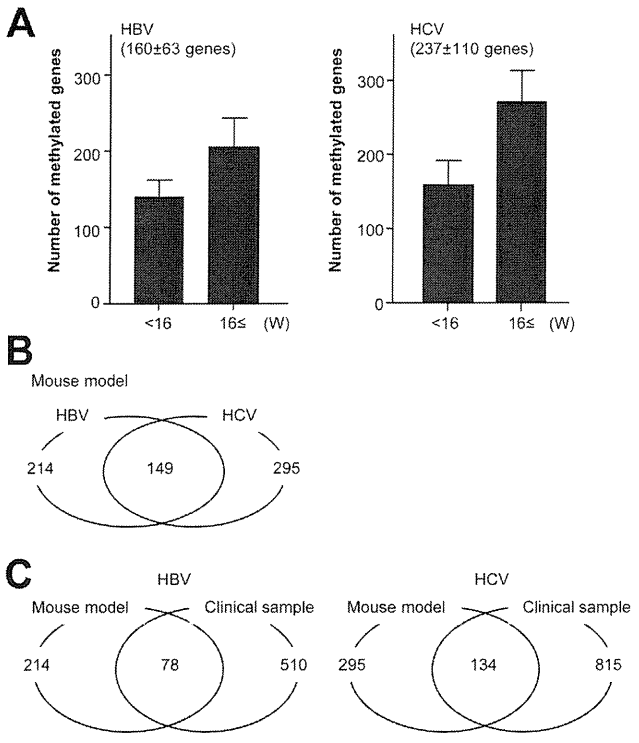

Figure 2. DNA methylation analysis in human hepatocyte chimeric mice with HBV or HCV infection. (*A*) The number of DNA methylation target genes in HBV mice and HCV mice by MCAM analysis. Error bars denote standard deviations. (*B*) The number of DNA methylation target genes in HBV mice and HCV mice is shown by Venn diagram. (*C*) The number of common DNA methylation target genes in the mouse model and clinical samples is shown by Venn diagram (*left*, HBV mice and HBV-associated clinical samples; *right*, HCV mice and HCV-associated clinical samples).

suppressor gene, DNA methylation of which has been shown to accumulate according to HCC progression.[8] Four (*RASSF1A, HOXA6, ESR1,* and *zinc finger protein 385A*) of 5 genes were moderately to highly methylated in the hepatocellular carcinoma cell line, Huh7.5.1 (Supplementary Table 5). Most of the 5 genes showed increased DNA methylation in a time-dependent manner during HBV or HCV infection (Figure 3*B*). Intriguingly, the DNA methylation level in 3 genes, *RASSF1A*, *ESR1*, and ELOVL fatty acid elongase 3, in uninfected mice (≥16 weeks) was slightly or moderately increased (13%, 29%, and 14%, respectively, Supplementary Table 5) as compared with unmethylated control DNA (normal lymphocyte DNA, 8%, 9%, and 7%, respectively). This was consistent with the MCAM data showing that the average signal intensity of Cy3 (DNA from uninfected mice) of the commonly methylated 149 genes in both HBV mice and HCV mice (Figure 2*B*) was significantly higher than that of other genes (Supplementary Figure 3). Given the principle of the MCAM technique, which allows for efficient polymerase chain reaction amplification of methylated CpG islands,[22] these data suggested that there were some genes that were methylated at low levels, even in normal tissues (eg, age-related DNA methylation) and were prone to DNA methylation in response to continuous viral infection regardless of viral types.[23] Conceivably, increased DNA methylation level in this model might not be due simply to the increased expression level of DNA methyltransferases or decreased level of methylcytosine dioxygenases, such as ten-eleven translocation 1 and 2, which are associated with DNA demethylation (Supplementary Figure 6)

Expression of Inflammation-Related Genes in Human Hepatocyte Chimeric Mice With HBV or HCV Infection

Our data in human hepatocyte chimeric mice suggested a link between activated host immune system by viral infection and induction of DNA methylation. We examined the kinetics of several inflammation-related genes, *Ifng*, *Il1b*, *Il6*, *Il12b*, *Tnf*, and *Cxcl2* using either mouse- or human-specific primer sets; among them IFN-gamma production was attributed to NK cells of SCID mice, and interleukin (IL)-1β, IL-6, IL-12, CXCL2, and tumor necrosis factor−α were produced by the other types of cells, such as Kupffer cells and hepatocytes.[24,25] In addition, the protein level of IFN-gamma from mouse-derived cells was evaluated by mouse-specific anti−IFN-gamma (Supplementary Figure 8*E*). The levels of these inflammation-related genes produced from human-derived cells were much lower than those produced from mouse-derived cells, indicating the predominant role of the mouse innate immune system against HBV or HCV infection in this mouse model (Supplementary Figure 4). Uninfected mice showed very low expression of the *Ifng* and *Il12b* genes in liver tissues, while *Il1b*, *Il6*, *Tnf*, and *Cxcl2* were substantially expressed. Expression levels of *Ifng* and *Tnf* significantly increased in both HBV- and HCV-infected livers ($P < .05$, Figure 4*A*). Expression level of *Il12b* was significantly increased in HCV-infected liver, and also tended to increase in HBV-infected liver, although the difference was not statistically significant. By contrast, expression levels of the 3 other genes, *Il1b*, *Il6*, and *Cxcl2*, did not significantly increase after viral infection. It appears that DNA methylation was not involved in the regulation of expression of those cytokines, because no aberrant DNA methylation was detected in the promoter regions of the corresponding genes (Supplementary Table 5). The induction of *Ifng* and *Il12b* genes was almost completely abolished by administration of a specific inhibitor of NK cell activity, anti−asialo GM-1 treatment.[26] However, the treatment of anti−asialo GM-1 did not significantly affect *Tnf* expression in HCV mice. In addition, this treatment showed no effect on virus levels in both HBV and HCV mice (Supplementary Figure 7).

Notably, IFN-gamma is known to enhance the production of ROS in inflammatory cells, such as activated Kupffer cells.[27,28] ROS production was evaluated by dihydroethidium staining (Figure 4*B*).[16] Quantification of fluorescence intensity in liver specimens revealed that the level of ROS production was significantly increased in both HBV and HCV mice in comparison with uninfected mice (Figure 4*C*; $P < .05$). Intriguingly, induction of ROS was abolished by anti−asialo GM-1 treatment, which confirmed that ROS

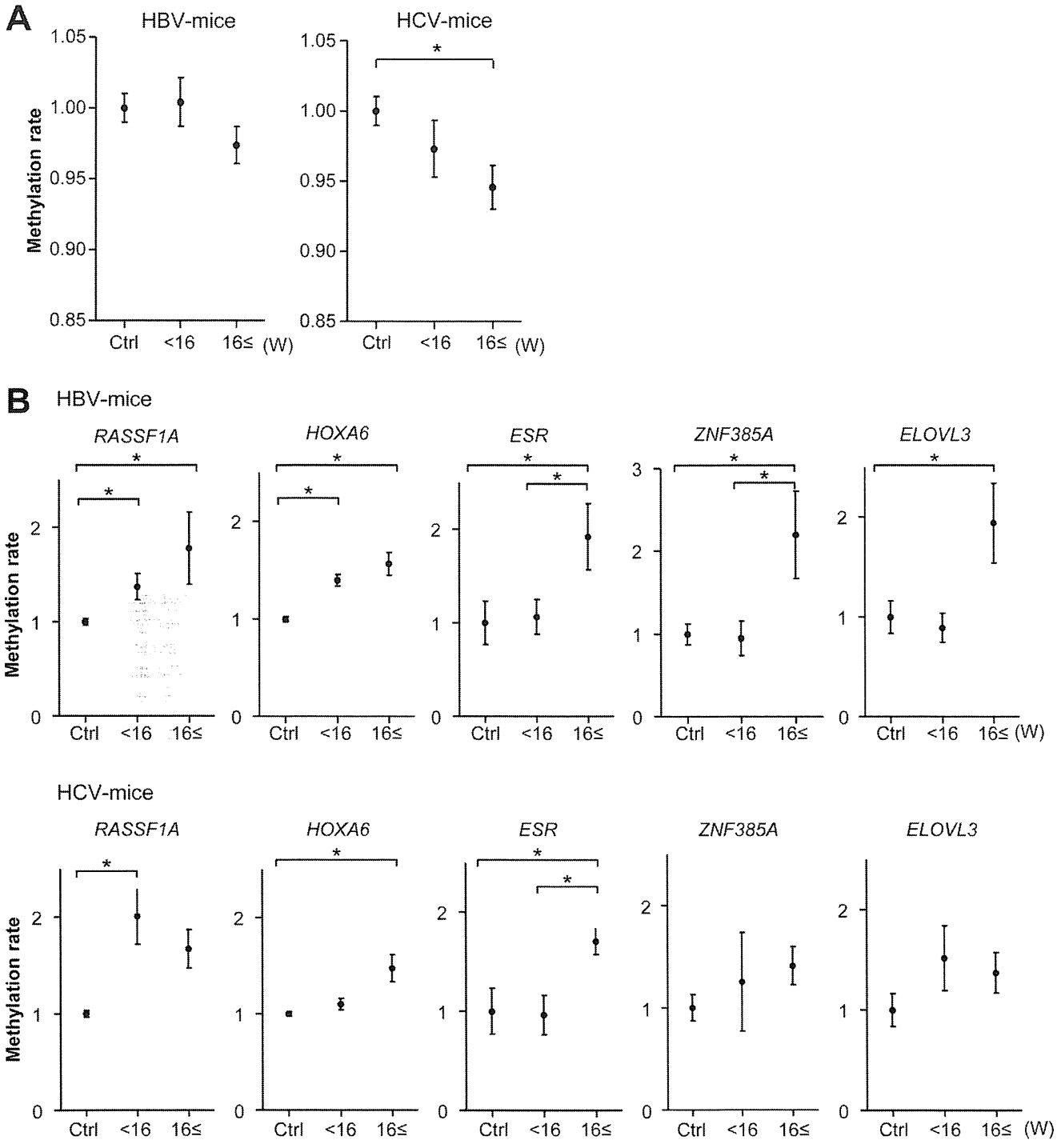

Figure 3. Time-dependent alterations in DNA methylation after HBV and HCV infections. DNA methylation levels of *LINE1* (*A*) and 5 target genes (*B*) in HBV mice and HCV mice by pyrosequencing analysis. Y-axis indicates relative values of DNA methylation level in HBV or HCV mice to that of uninfected mice. Error bars denote standard deviations. *$P < .05$. Ctrl, control; ELOVL3, ELOVL fatty acid elongase 3; ZNF385A, zinc finger protein 385A.

production after virus infection was dependent on NK cell activity. These dynamic changes in cytokine level and ROS production appeared to be reflected by the alanine aminotransferase level, especially in HBV mice (Supplementary Figure 7).

Evaluation of Cell Proliferation in Human Hepatocytes With Ki-67 and Proliferating Cell Nuclear Antigen After Viral Infection

When virus-infected hepatocytes are destroyed, hepatocyte regeneration is activated, resulting in continual

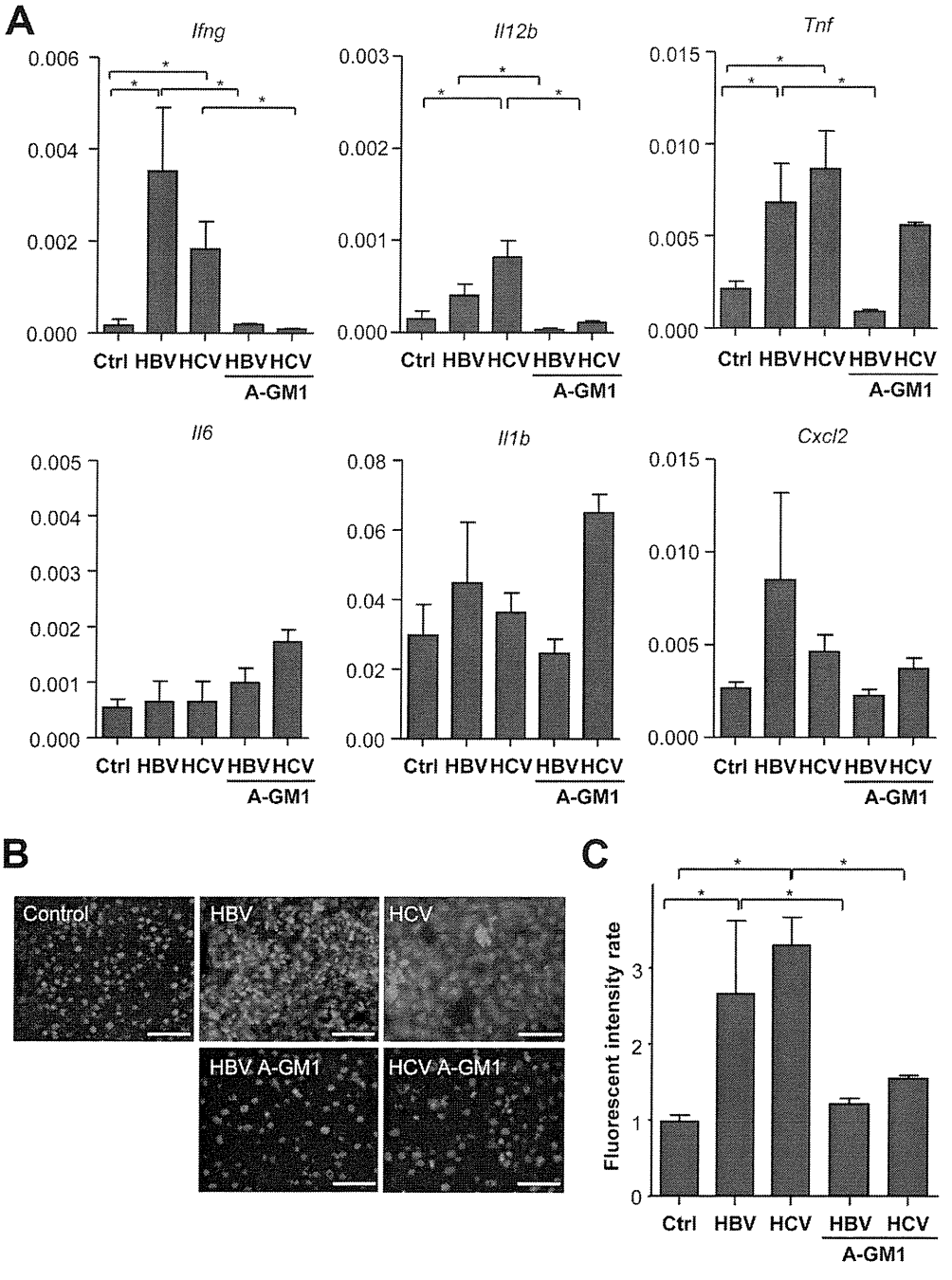

Figure 4. Expression analysis of inflammation-related genes in HBV and HCV mice. (*A*) Gene expression of *Ifng*, *Il12b*, *Tnf*, *Il1b*, *Il6*, and *Cxcl2* was measured by quantitative reverse transcription polymerase chain reaction in HBV and HCV mice with and without treatment of anti–asialo GM-1 (A-GM1) using mouse-specific primers. Relative values of messenger RNA expression for each gene normalized to *glyceraldehyde-3-phosphate dehydrogenase* are shown in Y-axis. Error bars denote standard deviations. $^*P < .05$. (*B*) Production of ROS was analyzed in liver sections of HBV and HCV mice with and without treatment of anti–asialo GM-1 by fluorescence microscopy. Bar = 50 μm. (*C*) Fluorescence intensity in different areas (at least 5 areas) of each image was quantified. Relative values of averaged intensities in HBV and HCV mice to uninfected control (Ctrl) are shown in Y-axis. Error bars denote standard deviations. $^*P < .05$.

proliferation of hepatocytes and constant liver regeneration.[29,30] In response to viral infection and activation of the innate immune system, expression of *NFKB1*, which enhances the proliferation of hepatocytes, was increased in human hepatocytes (Figure 5*A*). This induction was abolished by anti–asialo GM-1 treatment. We analyzed the Ki-67 index as a proliferation marker and found that it was increased in both HBV-infected and HCV-infected liver tissues as compared with uninfected control (P =.03, P =.006, respectively; Figure 5*B*). Consistently, a similar tendency was observed in the expression of another proliferation marker, proliferating cell nuclear antigen *(PCNA)* and in the bromodeoxyuridine uptake analysis as well (Figure 5*C* and *D*). The induction of *PCNA* or bromodeoxyuridine incorporation was also abolished by anti–asialo GM-1 treatment.

Inhibition of NK Cell Function by Anti–Asialo GM1 Attenuated the Induction of DNA Methylation in HBV and HCV Mice

NK cell activity can be almost completely abolished by administration of anti–asialo GM-1 treatment. To clarify

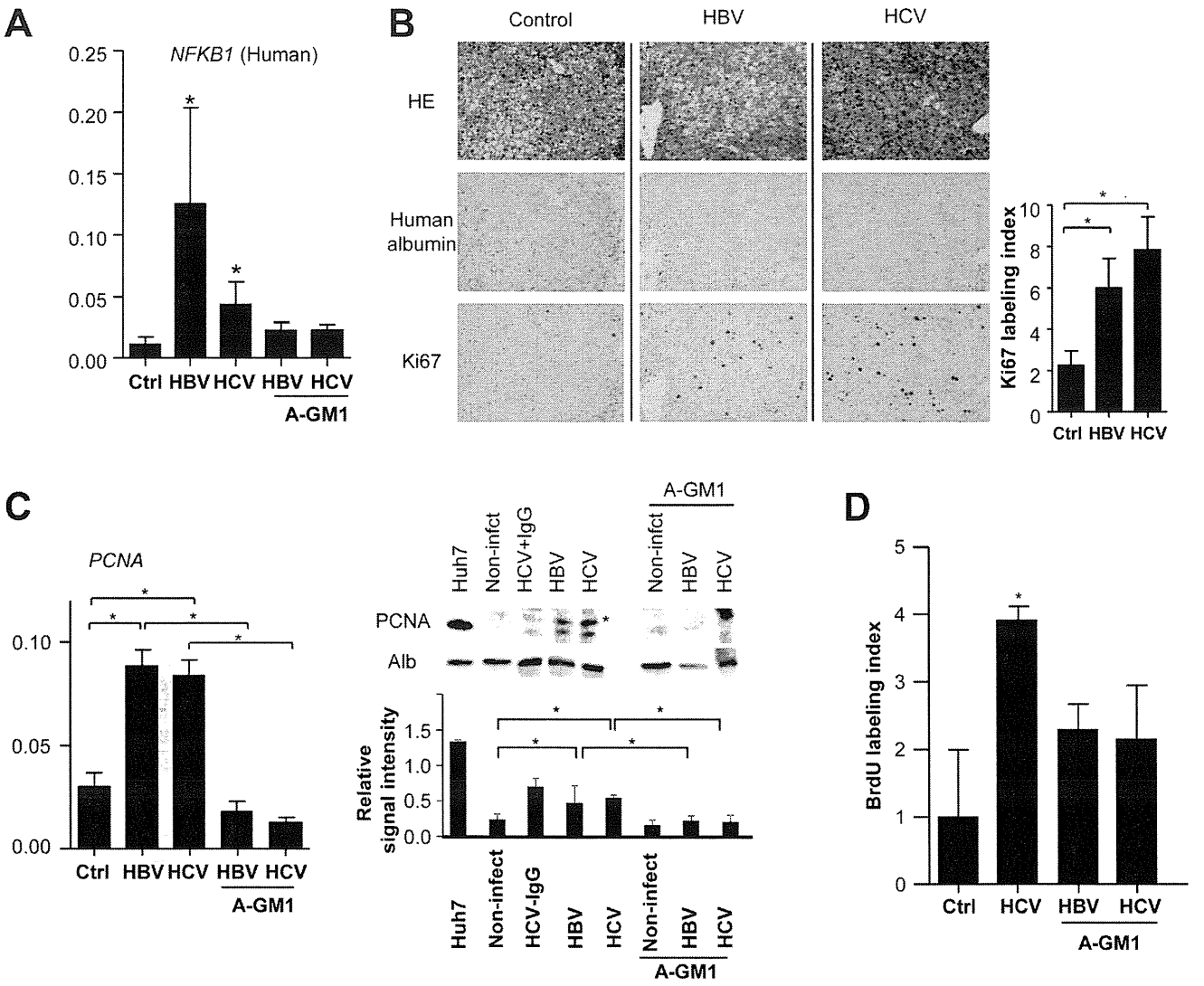

Figure 5. Evaluation of hepatocyte proliferation in HBV and HCV mice. (*A*) Expression of *NFKB1* was analyzed in HBV and HCV mice using human-specific primers. Expression of *NFKB1* in HBV and HCV mice without anti–asialo GM-1 treatment (A-GM1) was significantly higher than that in HBV and HCV mice with A-GM1 treatment (*$P < .05$). Error bars denote standard deviations. (*B*) Histologic comparison among uninfected, HBV, and HCV mice. Liver specimens stained with H&E, anti-human albumin, and anti-human Ki-67 are shown (*left panel*). Ki-67 labeling index was calculated and is shown in *bar graph* (*right panel*). (*C*) Expression of PCNA was analyzed by quantitative reverse transcription polymerase chain reaction using human-specific primers (*left panel*). *$P < .05$. Protein level of PCNA was examined by Western blotting (*right upper panel*) and band intensities were quantified (*right bottom panel*). IgG, nonspecific rabbit polyclonal antibody treatment. *Nonspecific bands are observed around 40 kDa. (*D*) Bromodeoxyuridine (BrdU) labeling index was calculated and is shown in *bar graph*.

whether attenuated NK cell activity affected DNA methylation status, we examined HBV and HCV mice with and without anti–asialo GM-1 treatment (Figure 6). In the context of global DNA methylation, the level of *LINE1*-methylation was decreased in HBV and HCV mice, and anti–asialo GM-1–treated mice showed sustained levels of *LINE*1 methylation. Consistently, anti–asialo GM-1 treatment attenuated the induction of DNA methylation in *RASSF1A*, *HOXA6*, and *ESR1* genes in HBV and HCV mice as well ($P < .05$, respectively).

In order to confirm whether NK cell activity via IFN-gamma is a major cause of induction of DNA methylation, we neutralized IFN-gamma activity using an anti-mouse IFN-gamma in the chimeric mice with and without virus infection (Supplementary Figure 8). Concordant with the anti–asialo GM-1 treatment, anti-mouse IFN-gamma blocked the induction of DNA methylation together with suppression of ROS production and hepatocyte cell proliferation, although the effects of anti–IFN-gamma were a little milder than those of anti–asialo GM-1 treatment.

Taken together, these data demonstrated that NK cell activity and its associated immune reaction were incriminated in induction of aberrant DNA methylation in human hepatocytes after viral infection.

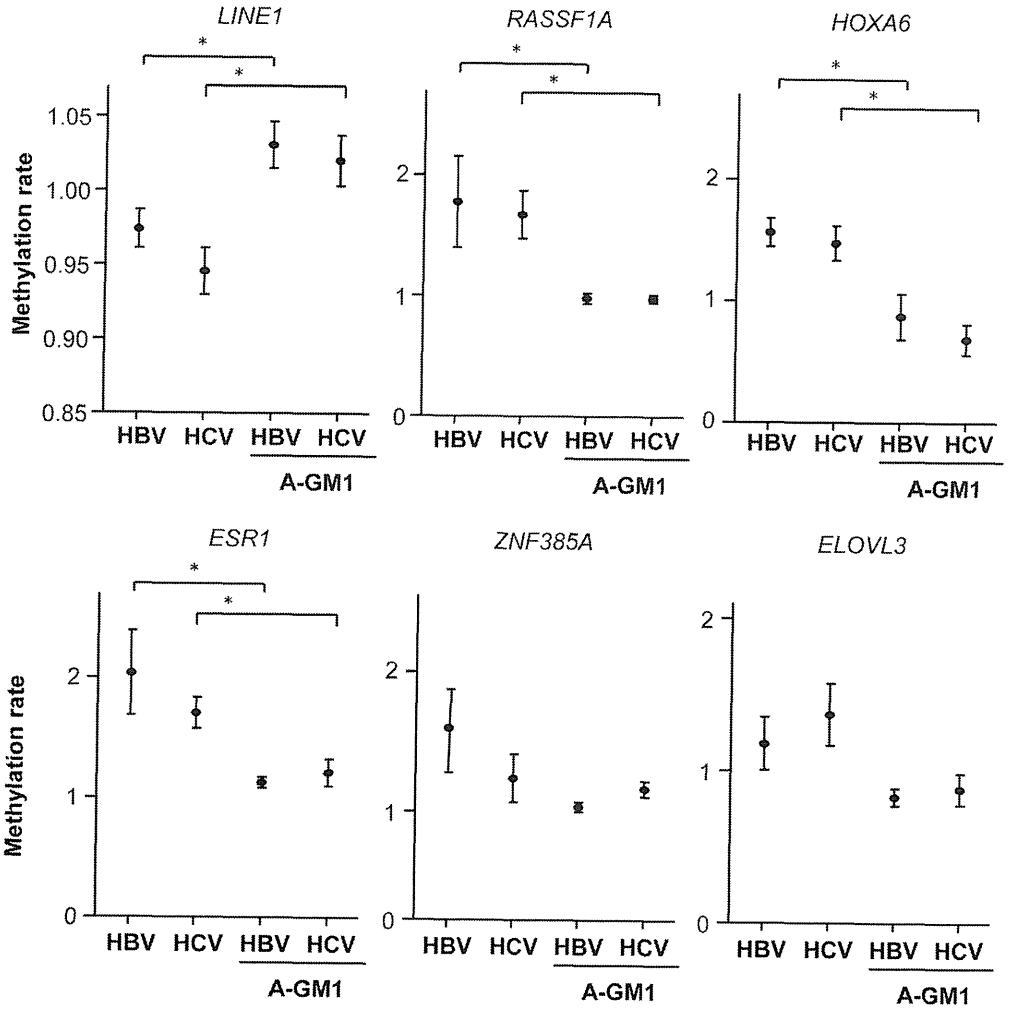

Figure 6. Levels of DNA methylation in HBV and HCV mice with and without treatment of anti–asialo GM1 (A-GM1). DNA methylation levels of *LINE1*, *RASSF1A*, *HOXA6*, *ESR1*, zinc finger protein 385A (*ZNF385A*), and ELOVL fatty acid elongase 3 (*ELOVL3*) genes in HBV and HCV mice with and without treatment of A-GM1 were analyzed by pyrosequencing analysis. Y-axis indicates the same as in Figure 3. *$P < .05$.

Discussion

In the current study, we examined the dynamics of DNA methylation after initial infection with HBV or HCV in hepatocytes using an in vivo human hepatocyte chimeric mouse model.[13,14,16] Using this model, we reproducibly found that genome-wide DNA methylation changes were induced in a time-dependent manner after viral infection, and no significant alterations in DNA methylation were induced in a tissue culture–based HCV infection model. Conceivably, the minimum effects on cell proliferation and moderate ROS production after in vitro HCV infection enabled induction of DNA methylation in Huh7.5.1 cells, in which the basal level of DNA methylation is already elevated.

Some of the DNA methylation target genes in human hepatocytes in HBV and HCV mice were comprised of well-known tumor suppressor genes (eg, *RASSF1A*), which were also methylated in clinical HCC cases, suggesting clinical relevance of this mouse model to study dynamics of DNA methylation after hepatitis virus infection.

Among the examined cytokine-associated genes, *Ifng* was significantly up-regulated in response to HBV and HCV infections. Typically, IFN-gamma is produced by NK cells and plays an important role in attenuating HBV and HCV pathogenesis during initial infection.[24,31] IFN-gamma potentially stimulates Kupffer cells and dendritic cells to produce an abundance of cytokines, including IL-12.[32,33] In addition to producing cytokines, Kupffer cells activated by IFN-gamma are the major source of ROS in the liver.[27,28] Intriguingly, IL-12 is a potent activator of NK cell effector function. This feedback loop can efficiently function to activate the innate immune system and induce NK cell–mediated liver damage. In our model, up-regulation of mouse-specific *Ifng* and *Il12b* was almost completely attenuated by treatment with anti–asialo GM1, together with sustained DNA methylation in several genes. These data indicated that in our mouse model, NK cell function was a key player in inducing aberrant DNA methylation in human hepatocytes after initial HBV and HCV infections. In line with our study, several studies have demonstrated that inflammation-associated mechanisms can induce aberrant DNA methylation in mouse epithelial cells of the stomach and colon in vivo.[34–36] In addition, a recent in vitro study showed that oxidative damage induces recruitment of DNA

methyltransferase in certain loci to promote aberrant DNA methylation.[37,38] In addition to these models, we propose here a possibility that aberrant DNA methylation accumulates via cell-cycle activities, which induce inappropriately accelerated aging in hepatocytes. A few lines of evidence support our hypothesis. When virus-infected hepatocytes are destroyed by immune reaction, such as by activated Kupffer cells, hepatocyte regeneration is generally activated; repeated cycles of immune-mediated clearance of virus-infected hepatocytes cause continual proliferation of hepatocytes and constant liver regeneration, which is modulated by nuclear factor–κB function.[29] We detected significantly increased cell proliferation coupled with nuclear factor–κB induction in HBV- and HCV-infected liver specimens in the mice. These phenomena might be connected with the replication-linked stochastic error model that predicts that variability first arises during aging and that cancers could accentuate variability.[23,39] Given that it can be seen even in normal aging tissues, this variation and the consequent natural selection are probably more obvious in highly proliferative conditions (eg, chronic hepatitis), resulting in their contribution to focal proliferative lesions, such as preneoplastic tumors. Large numbers of the DNA methylated genes after viral infection in the mouse model appeared to be age-related DNA methylation target genes. We propose that continuous inflammation and induction of certain types of cytokines in the liver can induce aberrant DNA methylation via increased cell turnover. Compellingly, recent clinical reports showing that the presence of hepatitis viruses, especially HCV, could play a role in accelerating the methylation process (age-related) that is involved in HCC development.[19] Although there is a weak inverse correlation between DNA methylation level and gene expression in the 5 genes examined, none of them were silenced (Supplementary Figure 6), suggesting that the accumulated DNA methylation level of each gene during the period of viral infection examined in this study was still not high enough to inactivate the gene expression.

In conclusion, this is the first study to show the initial dynamics of DNA methylation after HBV and HCV infections in human hepatocytes in an in vivo model. Multiple machineries, including DNA methyltransferase and oxidative stress, can induce DNA methylation; however, the current model convincingly showed that NK cell function and consequent mechanisms were the key factors for induction of DNA methylation. This model probably did not develop HCC due to limited observation time. Given the critical roles of epigenetic alterations in hepatocarcinogenesis after viral infection, control of inflammation, as well as key molecules such as IFN-gamma, are good potential targets for prevention of inflammation-associated cancer development.

Supplementary Material

Note: To access the supplementary material accompanying this article, visit the online version of *Gastroenterology* at www.gastrojournal.org, and at http://dx.doi.org/10.1053/j.gastro.2013.10.056.

References

1. Thorgeirsson SS, Grisham JW. Molecular pathogenesis of human hepatocellular carcinoma. Nat Genet 2002; 31:339–346.
2. Baylin SB, Herman JG, Graff JR, et al. Alterations in DNA methylation: a fundamental aspect of neoplasia. Adv Cancer Res 1998;72:141–196.
3. Jones PA, Baylin SB. The fundamental role of epigenetic events in cancer. Nat Rev Genet 2002;3:415–428.
4. Kondo Y, Kanai Y, Sakamoto M, et al. Genetic instability and aberrant DNA methylation in chronic hepatitis and cirrhosis—a comprehensive study of loss of heterozygosity and microsatellite instability at 39 loci and DNA hypermethylation on 8 CpG islands in microdissected specimens from patients with hepatocellular carcinoma. Hepatology 2000;32:970–999.
5. Yu J, Ni M, Xu J, et al. Methylation profiling of twenty promoter-CpG islands of genes which may contribute to hepatocellular carcinogenesis. BMC Cancer 2002;2:29.
6. Lee S, Lee HJ, Kim JH, et al. Aberrant CpG island hypermethylation along multistep hepatocarcinogenesis. Am J Pathol 2003;163:1371–1378.
7. Schagdarsurengin U, Wilkens L, Steinemann D, et al. Frequent epigenetic inactivation of the RASSF1A gene in hepatocellular carcinoma. Oncogene 2003;22: 1866–1871.
8. Gao W, Kondo Y, Shen L, et al. Variable DNA methylation patterns associated with progression of disease in hepatocellular carcinomas. Carcinogenesis 2008;29: 1901–1910.
9. Park IY, Sohn BH, Yu E, et al. Aberrant epigenetic modifications in hepatocarcinogenesis induced by hepatitis B virus X protein. Gastroenterology 2007;132: 1476–1494.
10. Jung JK, Arora P, Pagano JS, et al. Expression of DNA methyltransferase 1 is activated by hepatitis B virus X protein via a regulatory circuit involving the p16INK4a-cyclin D1-CDK 4/6-pRb-E2F1 pathway. Cancer Res 2007;67:5771–5778.
11. Zheng DL, Zhang L, Cheng N, et al. Epigenetic modification induced by hepatitis B virus X protein via interaction with de novo DNA methyltransferase DNMT3A. J Hepatol 2009;50:377–587.
12. Higgs MR, Lerat H, Pawlotsky JM. Downregulation of Gadd45beta expression by hepatitis C virus leads to defective cell cycle arrest. Cancer Res 2010;70: 4901–4911.
13. Mercer DF, Schiller DE, Elliott JF, et al. Hepatitis C virus replication in mice with chimeric human livers. Nat Med 2001;7:927–933.
14. Barth H, Robinet E, Liang TJ, et al. Mouse models for the study of HCV infection and virus-host interactions. J Hepatol 2008;49:134–142.
15. Meuleman P, Libbrecht L, De Vos R, et al. Morphological and biochemical characterization of a human liver in a uPA-SCID mouse chimera. Hepatology 2005;41: 847–856.
16. Sugiyama M, Tanaka Y, Kurbanov F, et al. Direct cytopathic effects of particular hepatitis B virus genotypes in

severe combined immunodeficiency transgenic with urokinase-type plasminogen activator mouse with human hepatocytes. Gastroenterology 2009;136:652–662 e3.
17. **Wakita T, Pietschmann T**, Kato T, et al. Production of infectious hepatitis C virus in tissue culture from a cloned viral genome. Nat Med 2005;11:791–796.
18. Choudhry N, Petry F, van Rooijen N, et al. A protective role for interleukin 18 in interferon gamma-mediated innate immunity to Cryptosporidium parvum that is independent of natural killer cells. J Infect Dis 2012; 206:117–124.
19. Nishida N, Nagasaka T, Nishimura T, et al. Aberrant methylation of multiple tumor suppressor genes in aging liver, chronic hepatitis, and hepatocellular carcinoma. Hepatology 2008;47:908–918.
20. Zhong J, Gastaminza P, Cheng G, et al. Robust hepatitis C virus infection in vitro. Proc Natl Acad Sci U S A 2005; 102:9294–9299.
21. Yang AS, Estecio MR, Doshi K, et al. A simple method for estimating global DNA methylation using bisulfite PCR of repetitive DNA elements. Nucleic Acids Res 2004;32:e38.
22. Toyota M, Ho C, Ahuja N, et al. Identification of differentially methylated sequences in colorectal cancer by methylated CpG island amplification. Cancer Res 1999; 59:2307–2312.
23. Issa JP. Epigenetic variation and cellular Darwinism. Nat Genet 2011;43:724–726.
24. Rehermann B, Nascimbeni M. Immunology of hepatitis B virus and hepatitis C virus infection. Nat Rev Immunol 2005;5:215–229.
25. **Krohn N, Kapoor S**, Enami Y, et al. Hepatocyte transplantation-induced liver inflammation is driven by cytokines-chemokines associated with neutrophils and Kupffer cells. Gastroenterology 2009;136:1806–1817.
26. Kasai M, Yoneda T, Habu S, et al. In vivo effect of anti-asialo GM1 antibody on natural killer activity. Nature 1981;291:334–335.
27. **Watanabe Y, Suzuki O**, Haruyama T, et al. Interferon-gamma induces reactive oxygen species and endoplasmic reticulum stress at the hepatic apoptosis. J Cell Biochem 2003;89:244–253.
28. Wheeler MD. Endotoxin and Kupffer cell activation in alcoholic liver disease. Alcohol Res Health 2003;27: 300–306.
29. Berasain C, Castillo J, Perugorria MJ, et al. Inflammation and liver cancer: new molecular links. Ann N Y Acad Sci 2009;1155:206–221.
30. Bouchard MJ, Navas-Martin S. Hepatitis B and C virus hepatocarcinogenesis: lessons learned and future challenges. Cancer Lett 2011;305:123–143.
31. Horras CJ, Lamb CL, Mitchell KA. Regulation of hepatocyte fate by interferon-gamma. Cytokine Growth Factor Rev 2011;22:35–43.
32. Wullaert A, van Loo G, Heyninck K, et al. Hepatic tumor necrosis factor signaling and nuclear factor-kappaB: effects on liver homeostasis and beyond. Endocr Rev 2007;28:365–386.
33. Vivier E, Tomasello E, Baratin M, Walzer T, Ugolini S. Functions of natural killer cells. Nat Immunol 2008;9:503–510.
34. Niwa T, Tsukamoto T, Toyoda T, et al. Inflammatory processes triggered by Helicobacter pylori infection cause aberrant DNA methylation in gastric epithelial cells. Cancer Res 2010;70:1430–1440.
35. Hur K, Niwa T, Toyoda T, et al. Insufficient role of cell proliferation in aberrant DNA methylation induction and involvement of specific types of inflammation. Carcinogenesis 2012;32:35–41.
36. Katsurano M, Niwa T, Yasui Y, et al. Early-stage formation of an epigenetic field defect in a mouse colitis model, and non-essential roles of T- and B-cells in DNA methylation induction. Oncogene 2012;31:342–351.
37. **O'Hagan HM, Wang W**, Sen S, et al. Oxidative damage targets complexes containing DNA methyltransferases, SIRT1, and polycomb members to promoter CpG Islands. Cancer Cell 2011;20:606–619.
38. Lim SO, Gu JM, Kim MS, et al. Epigenetic changes induced by reactive oxygen species in hepatocellular carcinoma: methylation of the E-cadherin promoter. Gastroenterology 2008;135:2128–2140, 2140 e1–8.
39. **Hansen KD, Timp W, Bravo HC, et al.** Increased methylation variation in epigenetic domains across cancer types. Nat Genet 2011;43:768–775.

Author names in bold designate shared co-first authorship.

Received February 12, 2013. Accepted October 24, 2013.

Reprint requests
Address requests for reprints to: Yutaka Kondo, MD, PhD, Division of Epigenomics, Aichi Cancer Center Research Institute, 1-1 Kanokoden, Chikusa-ku, Nagoya 464-8681, Japan. e-mail: ykondo@aichi-cc.jp; fax: +81-52-764-2994.

Acknowledgments
The authors would like to thank Ms Ikuko Tomimatsu for technical assistance. ArrayExpress accession (http://www.ebi.ac.uk/arrayexpress/): E-MTAB-1472, E-MTAB-1473, E-MTAB-1474.

Conflicts of interest
The authors disclose no conflicts.

Funding
This work was supported by Grants-in-Aid for Cancer Research (15-20 and 19-17) from the Ministry of Health, Labour and Welfare and a grant from the Japan Society for the Promotion of Science, PRESTO of JST (YK), Grant-in-Aid for Scientific Research from the Japan Society for the Promotion of Science (YK, YT, and YO), the Uehara Memorial Foundation (YK), Takeda Science Foundation (YK).

Published OnlineFirst January 27, 2014; DOI: 10.1158/2159-8290.CD-13-0633

CANCER DISCOVERY

CD74–NRG1 Fusions in Lung Adenocarcinoma

Lynnette Fernandez-Cuesta, Dennis Plenker, Hirotaka Osada, et al.

Cancer Discovery 2014;4:415-422. Published OnlineFirst January 27, 2014.

Published OnlineFirst January 27, 2014; DOI: 10.1158/2159-8290.CD-13-0633

RESEARCH BRIEF

CD74–NRG1 Fusions in Lung Adenocarcinoma

Lynnette Fernandez-Cuesta[1], Dennis Plenker[1], Hirotaka Osada[19], Ruping Sun[13], Roopika Menon[9,14], Frauke Leenders[1,3], Sandra Ortiz-Cuaran[1], Martin Peifer[1,5], Marc Bos[1], Juliane Daßler[15], Florian Malchers[1], Jakob Schöttle[1,10], Wenzel Vogel[14], Ilona Dahmen[1], Mirjam Koker[1], Roland T. Ullrich[2,10], Gavin M. Wright[21], Prudence A. Russell[22], Zoe Wainer[21], Benjamin Solomon[23], Elisabeth Brambilla[24], Hélène Nagy-Mignotte[25], Denis Moro-Sibilot[25], Christian G. Brambilla[25], Sylvie Lantuejoul[24], Janine Altmüller[6,7,12], Christian Becker[6], Peter Nürnberg[5,6,7], Johannes M. Heuckmann[9], Erich Stoelben[11], Iver Petersen[16], Joachim H. Clement[17], Jörg Sänger[18], Lucia A. Muscarella[26], Annamaria la Torre[26], Vito M. Fazio[26,27], Idoya Lahortiga[28], Timothy Perera[29], Souichi Ogata[29], Marc Parade[29], Dirk Brehmer[29], Martin Vingron[13], Lukas C. Heukamp[8], Reinhard Buettner[3,4,8], Thomas Zander[1,2,4], Jürgen Wolf[2,3,4], Sven Perner[14], Sascha Ansén[2], Stefan A. Haas[13], Yasushi Yatabe[20], and Roman K. Thomas[1,3,8]

ABSTRACT We discovered a novel somatic gene fusion, *CD74–NRG1*, by transcriptome sequencing of 25 lung adenocarcinomas of never smokers. By screening 102 lung adenocarcinomas negative for known oncogenic alterations, we found four additional fusion-positive tumors, all of which were of the invasive mucinous subtype. Mechanistically, CD74–NRG1 leads to extracellular expression of the EGF-like domain of NRG1 III-β3, thereby providing the ligand for ERBB2–ERBB3 receptor complexes. Accordingly, ERBB2 and ERBB3 expression was high in the index case, and expression of phospho-ERBB3 was specifically found in tumors bearing the fusion ($P < 0.0001$). Ectopic expression of CD74–NRG1 in lung cancer cell lines expressing ERBB2 and ERBB3 activated ERBB3 and the PI3K–AKT pathway, and led to increased colony formation in soft agar. Thus, *CD74–NRG1* gene fusions are activating genomic alterations in invasive mucinous adenocarcinomas and may offer a therapeutic opportunity for a lung tumor subtype with, so far, no effective treatment.

SIGNIFICANCE: *CD74–NRG1* fusions may represent a therapeutic opportunity for invasive mucinous lung adenocarcinomas, a tumor with no effective treatment that frequently presents with multifocal unresectable disease. *Cancer Discov; 4(4); 415–22. ©2014 AACR.*

Authors' Affiliations: [1]Department of Translational Genomics; [2]Department I of Internal Medicine; [3]Laboratory of Translational Cancer Genomics; [4]Network Genomic Medicine, University Hospital Cologne, Center of Integrated Oncology Cologne-Bonn; [5]Center for Molecular Medicine Cologne (CMMC); [6]Cologne Center for Genomics (CCG); [7]Cologne Excellence Cluster on Cellular Stress Responses in Aging-Associated Diseases (CECAD); [8]Department of Pathology, University Hospital Medical Center, University of Cologne; [9]Blackfield AG; [10]Max Planck Institute for Neurological Research; [11]Thoracic Surgery, Lungenklinik Merheim, Kliniken der Stadt Köln gGmbH; [12]Institute of Human Genetics, Cologne; [13]Computational Molecular Biology Department, Max Planck Institute for Molecular Genetics, Berlin; [14]Department of Prostate Cancer Research, Institute of Pathology; [15]Institute for Clinical Chemistry and Clinical Pharmacology, University Hospital Bonn, Bonn; [16]Institute of Pathology; [17]Department of Internal Medicine II, Jena University Hospital, Friedrich-Schiller-University, Jena; [18]Institute for Pathology Bad Berka, Bad Berka, Germany; [19]Division of Molecular Oncology, Aichi Cancer Center Research Institute; [20]Department of Pathology and Molecular Diagnostics, Aichi Cancer Center, Nagoya, Japan; Departments of [21]Surgery and [22]Pathology, St. Vincent's Hospital; [23]Department of Haematology and Medical Oncology, Peter MacCallum Cancer Centre, Melbourne, Victoria, Australia; [24]Department of Pathology, [25]CHU Grenoble Institut National de la Santé et de la Recherche Medicale (INSERM) U823, Institute Albert Bonniot, Grenoble-Alpes University, Grenoble, France; [26]Laboratory of Oncology IRCCS Casa Sollievo della Sofferenza, San Giovanni Rotondo; [27]Laboratory for Molecular Medicine and Biotechnology, University Campus Bio-Medico, Rome, Italy; [28]Center for the Biology of Disease, VIB, Leuven; and [29]Oncology Discovery, Janssen Research and Development, A Division of Janssen Pharmaceutica NV, Beerse, Belgium

Note: Supplementary data for this article are available at Cancer Discovery Online (http://cancerdiscovery.aacrjournals.org/).

L. Fernandez-Cuesta and D. Plenker contributed equally to this work.

Corresponding Author: Roman K. Thomas, Department of Translational Genomics, Medical Faculty, University of Cologne, Weyertal 115b, 50931 Cologne, Germany. Phone: 49-221-478-98771; Fax: 49-221-478-97902; E-mail: roman.thomas@uni-Koeln.de

doi: 10.1158/2159-8290.CD-13-0633

Published OnlineFirst January 27, 2014; DOI: 10.1158/2159-8290.CD-13-0633

INTRODUCTION

Lung adenocarcinomas of patients who have never smoked frequently bear kinase gene alterations, such as *EGFR* mutations and translocations affecting *ALK*, *ROS1*, and *RET* (1–6). These alterations cause "oncogene dependency" on the activated kinase and, thus, sensitivity of the tumor cells to kinase inhibitors. Patients whose tumors bear kinase gene alterations can be effectively treated with an ever-growing number of kinase inhibitors; for example, patients with *EGFR*-mutant lung cancer treated with EGF receptor (EGFR) inhibitors have a significantly longer progression-free survival compared with patients treated with conventional chemotherapy (7). Similarly, ALK and ROS1 inhibition induces clinically relevant remissions in patients bearing the respective genomic fusion (8–10). Unfortunately, despite substantive cancer genome sequencing efforts, a majority of lung tumors still lack therapeutically tractable kinase alterations (1). We therefore sought to identify novel therapeutically relevant driver alterations in otherwise driver-negative lung adenocarcinomas.

RESULTS

We collected a cohort of 25 lung adenocarcinoma specimens of never smokers that lacked mutations in *KRAS* or *EGFR*, on which we performed chromosomal gene copy-number analysis as well as transcriptome sequencing with the aim of identifying new oncogenic driver alterations. We applied a novel computational data analysis strategy that combines split-read and read-pair analyses with *de novo* assembly of candidate regions containing potential breakpoints to achieve sensitive and accurate detection of fusion transcripts (see Methods; Fernandez-Cuesta and colleagues, published elsewhere). Of the 25 samples analyzed (Supplementary Table S1), 10 carried a known oncogene. One sample exhibited *EGFR* amplification, paralleled by overexpression of the gene (Fig. 1A and Supplementary Fig. S1). We also found 3 cases each of *ALK*, *ROS1*, and *RET* fusions (Fig. 1A and Supplementary Table S2). In addition, we detected one sample carrying a novel chimeric transcript fusing the first six exons of *CD74* to the exons encoding the EGF-like domain of the neuregulin-1 (NRG1) III-β3 isoform (Fig. 1A and B and Supplementary Table S2). This fusion raised our interest because *CD74* is part of recurrent fusions affecting the *ROS1* (3) kinase in lung adenocarcinoma, and because *NRG1* encodes a ligand of ERBB receptor tyrosine kinases, which are also frequently affected by genome alterations in this tumor type. NRG1 provides the ligand for ERBB3 and ERBB4 receptors (11). The NRG1 isoform present in our fusion transcript belongs to the type III and carries the EGF-like domain type β, which has higher affinity to the receptors than the α-type (12). NRG1 type III expression is mostly limited to neurons and is the only isoform displaying this degree of tissue-specific expression (13). Only the sample carrying the *CD74–NRG1* fusion exhibited high expression of the NRG1 III-β3 isoform [74 fragments per kilobase per million reads (FPKM); Fig. 1C, top; Supplementary Table S3], and in this specimen there was no expression of the wild-type allele (Fig. 1C, bottom). In addition, NRG1 was generally not expressed in lung adenocarcinoma as shown by transcriptome sequencing data of our cohort of 25 lung adenocarcinomas of never smokers (Fig. 1C, top, and Supplementary Table S3), and of a cohort of 15 unselected lung adenocarcinomas (Fig. 1C, top, and Supplementary Table S4). The fusion resulted from a somatic genomic event as *CD74–NRG1* fusion FISH and *NRG1* break-apart FISH revealed rearrangements in the respective chromosomal regions in the tumor cells, but not in surrounding nontumoral cells (Fig. 1D and Supplementary Fig. S2). Furthermore, by applying hybrid-capture–based massively parallel genomic sequencing (Fig. 1D and Supplementary Table S5), we found five and two reads spanning and encompassing the chromosomal breakpoint (chr5:149,783,493 and chr8:32,548,502), respectively.

We next performed reverse transcriptase PCR (RT-PCR) using primers specific for the chimeric transcript to identify additional tumors bearing the fusion in a set of 102 pan-negative adenocarcinomas of never smokers (wild-type for *EGFR*, *KRAS*, *BRAF*, *ERBB2*, *ALK*, *ROS*, and *RET* genes). We identified four additional tumors carrying the fusion (Supplementary Table S6), which were also confirmed by break-apart FISH. All 5 cases (including the index case) occurred in invasive mucinous adenocarcinomas (IMA) of women who had never smoked (Fig. 2A). Invasive mucinous lung adenocarcinoma is highly associated with *KRAS* mutations (14). Indeed, out of 15 invasive mucinous lung adenocarcinoma specimens (all derived from an East Asian population), six carried a *KRAS* mutation (40%), and four carried the *CD74–NRG1* fusion (27%; Fig. 2B; Supplementary Table S7). We additionally tested other lung tumor subtypes (63 cases), as well as four other cancer types (21 cases) and all were negative for the fusion gene (Supplementary Table S6), suggesting a strong link between the presence of *CD74–NRG1* and invasive mucinous adenocarcinoma.

Characteristic features of type III NRG1 are cytosolic N-termini and membrane-tethered EGF-like domains (13, 15). In the case of CD74–NRG1, the part of CD74 is predicted to replace the transmembrane domain present in wild-type NRG1 III-β3, preserving the membrane-tethered EGF-like domain (Fig. 2C). To validate this prediction, we transduced NIH-3T3 cells with CD74–NRG1-encoding retroviruses, and performed flow cytometry analyses to determine the subcellular distribution of expression of the fusion protein. As expected, we observed a positive intracellular (but not extracellular) signal for CD74 (Fig. 2D, left) and a positive extracellular signal for NRG1 (Fig. 2D, right). Similar results were observed in H2052 cells (Supplementary Fig. S3). Furthermore, we were unable to detect the fusion in the supernatant of transduced cells with a polyclonal antibody raised against the EGF-like domain (data not shown). Thus, the fusion does not lead to secretion of the EGF-like domain, but probably generates a membrane-bound protein with the EGF-like domain presented on the outside of the cell.

We next analyzed the expression of ERBB receptors in the index case: *ERBB1* (*EGFR*) was almost not expressed (FPKM = 1.9; Fig. 3A; Supplementary Table S8; Supplementary Fig. S4) and not phosphorylated (Supplementary Fig. S4). In contrast, *ERBB2* was expressed (FPKM = 22.9; Fig. 3A; Supplementary Table S8) and phosphorylated (Fig. 3B, left); similar to *ERBB2*, *ERBB3* was also expressed at relatively high levels

Published OnlineFirst January 27, 2014; DOI: 10.1158/2159-8290.CD-13-0633

A

Sample	Age	Sex	Stage	Driver
Case-01	63	Female	Ia	*EGFR*-amp
Case-08	68	Male	Ia	*EML4–ALK*
Case-10	46	Female	Ia	*EML4–ALK*
Case-17	39	Female	IIIa	*EML4–ALK*
Case-06	56	Female	IIIb	*CD74–ROS1*
Case-09	60	Female	Ia	*CD74–ROS1*
Case-02	68	Female	IIIb	*EZR–ROS1*
Case-15	65	Female	IIa	*KIF5B–RET*
Case-25	75	Male	Ia	*KIF5B–RET*
Case-23	66	Female	IIIb	*CCDC6–RET*
Case-19*	64	Female	Ib	*CD74–NRG1*
Case-03	72	Female	IV	
Case-04	74	Male	IV	
Case-05	50	Female	IV	
Case-07	70	Female	Ia	
Case-11	79	Female	IIa	
Case-12	72	Male	IV	
Case-13	59	Male	Ib	Unknown
Case-14	63	Female	IIIa	
Case-16	48	Male	IIIb	
Case-18	71	Female	IIIa	
Case-20	74	Female	IIIa	
Case-21	73	Male	Ib	
Case-22	80	Female	Ib	
Case-24	66	Female	IIIa	

*, Index case (Caucasian, invasive mucinous adenocarcinoma)

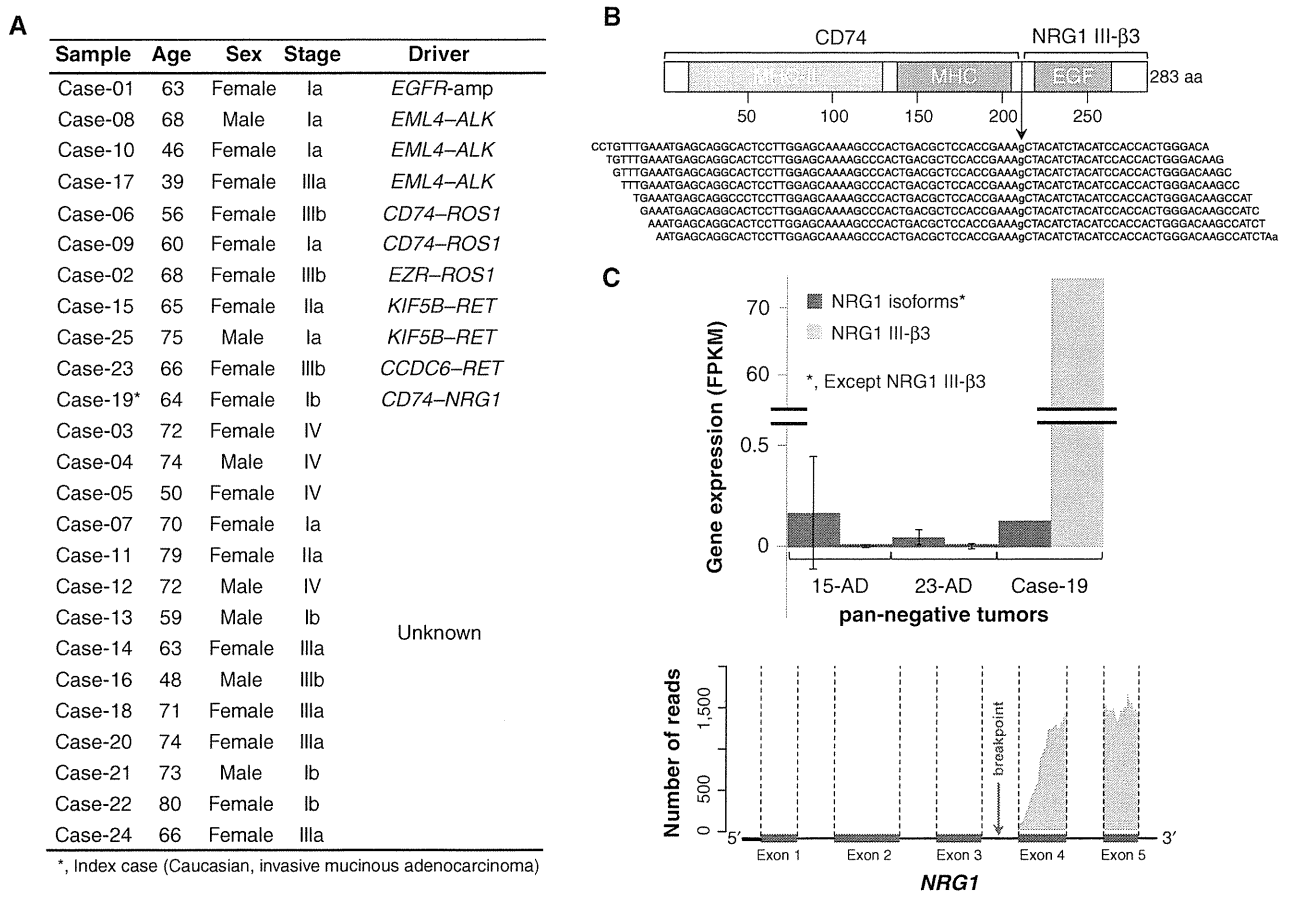

Figure 1. Identification of the *CD74-NRG1* fusion gene. **A,** overview of driver genes detected in a cohort of 25 *EGFR*- and *KRAS*-negative lung adenocarcinomas of never smokers. **B,** detection of *CD74-NRG1* fusion transcript by transcriptome sequencing. Schematic representation of the fusion transcript domains and some of the transcriptome sequencing reads spanning the fusion point. **C,** expression levels of *NRG1* isoforms in 15 unselected and 23 pan-negative lung adenocarcinomas (AD; wild-type for *EGFR*, *KRAS*, *BRAF*, *ERBB2*, *ALK*, *ROS*, and *RET*), and, in the index case, inferred from transcriptome sequencing data. Average FPKM values are shown (top). RNAseq analysis for *NRG1* reads to show where the breakpoint of *CD74-NRG1* occurs. The dip in exon 4 represents reads of the fusion that could not be mapped. No reads could be mapped to exons 1–3 (bottom). **D,** top, the genomic intron/exon structure of the *CD74* (in green) and the *NRG1* locus (in orange) with the genomic breakpoints marked in red. Sequencing reads were obtained from hybrid-capture–based genomic sequencing of 333 genes using genomic DNA of the index case (see Methods). The breakpoint-spanning reads are shown by means of the Integrative Genomics Viewer (www.broadinstitute.org/igv/) focused on the *CD74* gene (bottom). The gray area of the read is aligned to the *CD74* reference sequence. Colored area on the right indicates bases not matching the *CD74* reference sequence. Sequence comparison reveals alignment to the *NRG1* reference sequence. Encompassing reads whose mate pairs are mapped to the *NRG1* locus on chromosome 8 are displayed in dark purple. Bottom, a representative picture of *NRG1* break-apart FISH. Arrows, break-apart signals.